

26 **Address for correspondence:**

27 Dr Liku B Tezera

28 Clinical and Experimental Sciences

29 University of Southampton, Southampton SO16 1YD

30 Tel.: 00 44 23 8079 6671

31 E-mail: l.tezera@soton.ac.uk

32

33 **Running title:** PD-1 inhibition and TB reactivation

34

35

36 **Abstract**

37

38 Previously, we developed a 3-dimensional cell culture model of human tuberculosis (TB) and
39 demonstrated its potential to interrogate the host-pathogen interaction (Tezera et al, 2017).

40 Here, we use the model to investigate mechanisms whereby immune checkpoint therapy for
41 cancer paradoxically activates TB infection. In patients, PD-1 is expressed in *Mycobacterium*
42 *tuberculosis* (Mtb)-infected lung tissue but absent in areas of immunopathology. In the
43 microsphere model, PD-1 ligands are up-regulated by infection, and the PD-1/PD-L1 axis is
44 further induced by hypoxia. Inhibition of PD-1 signalling increases Mtb growth, and
45 augments cytokine secretion. TNF- α is responsible for accelerated Mtb growth, and TNF- α
46 neutralisation reverses augmented Mtb growth caused by anti-PD-1 treatment. In human TB,
47 pulmonary TNF- α immunoreactivity is increased and circulating PD-1 expression negatively
48 correlates with sputum TNF- α concentrations. Together, our findings demonstrate that PD-1
49 regulates the immune response in TB, and inhibition of PD-1 accelerates Mtb growth via
50 excessive TNF- α secretion.

51

52 **Introduction**

53

54 Tuberculosis (TB) continues to be a global health pandemic, killing more people than any
55 other infection (1). TB involves a complex host-pathogen interaction, with humans and
56 *Mycobacterium tuberculosis* (Mtb) having undergone prolonged co-evolution (2). TB has
57 often been thought to primarily result from loss of immune control, because approximately
58 90% individuals infected with TB never progress to active disease, and this progression is
59 increased in the context of immune deficiency; such as in cases of HIV infection, in infants,
60 people with genetic deficiency of the IL-12/IFN- γ signalling pathway or after anti-TNF- α
61 antibody treatment (3). However, an emerging concept is that an excessive immune response
62 to Mtb may be equally harmful. Standard disease paradigms predict that immune activation
63 resulting from the administration of checkpoint inhibitors should lead to better control of Mtb
64 infection (4). However, counter-intuitively these agents seem to be activating TB, as
65 evidenced by recent reports of TB developing in patients treated for malignancy with immune
66 checkpoint inhibition, often rapidly after commencing therapy (5-15). Consistent with this
67 emerging clinical phenomenon, programmed death (PD-1) deficient mice are highly
68 susceptible to TB, dying more rapidly than T-cell deficient mice (16, 17).

69

70 PD-1 and its ligand PD-L1 are expressed in human granulomas (10), suggesting a regulatory
71 role at the site of disease. TB granulomas are hypoxic (18), and PD-L1 is up-regulated by
72 hypoxia (19), further suggesting a mechanistic link between hypoxia and the PD-1/PD-L1
73 axis within TB lesions. In this study, we investigate the expression patterns of PD-1 and
74 PDL-1 within TB infected human lung tissue and the relationship between PD-1 and anti-TB
75 immunity. Next, using a human 3D cell culture model of TB (20), we show that hypoxia
76 increases expression of PD-1 and its ligands, that PD-1 inhibition increases Mtb growth.

77 Surprisingly, TNF- α is primarily responsible for this effect, and TNF- α neutralisation
78 reverses the anti-PD-1 induced phenotype.

79

80 **Results**

81

82 **PD-1 is expressed in human TB granulomas but not in areas of immunopathology**

83 First, we investigated the presence and localisation of PD-1-expressing T cells in human
84 pulmonary TB. We hypothesised that PD-1 would be expressed by T cells in the lung of
85 patients with TB, and at a higher frequency than in the blood. In thirty-five patients
86 undergoing medically indicated lung resection to treat TB or TB sequelae, PD-1 expression
87 was measured on T cells isolated from the lung and matched blood samples, available for 23
88 patients, by flow cytometry. Overall, PD-1 expression in homogenized lung tissue was highly
89 variable, with a trend towards increased PD-1 in both CD4 and CD8 T-cells from the lung
90 compared to matched blood, which reached statistical significance for CD8 T-cells (Figure
91 1A). Lung tissue from healthy individuals was not available for study, however, the median
92 frequency of 11 and 14% of PD-1 +ve CD4 and CD8 T-cells observed are generally lower
93 than recently reported for healthy human lung tissue from organ donors of approximately
94 50% for both cell types (21). As lung tissue is highly perfused with blood, distinguishing
95 cells of lung or blood origin is challenging.

96

97 To explore this further, we stained lung samples for canonical markers of tissue resident T-
98 cells, CD69 and CD103 (21). PD-1 expression on lung CD4 cells was predominantly
99 restricted CD69+ve T-cells, with a smaller proportion also expressing CD103 (Fig.1B,
100 overall frequencies Supplemental file 1), consistent with a tissue resident phenotype and in
101 contrast to PD-1 expressing cells in blood, which are largely CD69 negative (Figure 1–figure

102 supplement 1). Lung CD8 T-cells were also found to predominantly express CD69 in
103 addition to CD103, again in contrast to CD8 T-cells in circulation. Therefore, these data are
104 consistent with expression of PD-1 on lung tissue resident T-cells in patients with active or
105 previous pulmonary TB infection. However, TB immunopathology is highly heterogenous
106 within the lung and these analyses do not provide information as to the localization of PD-1
107 expression within TB lesions.

108

109 To address this question, we performed immunohistochemical analysis of human lung
110 biopsies of patients with active TB. Within stable granulomas with an intact cellular
111 structure, PD-1 expression was present around the central macrophage core (Figure 1C-i).
112 Both CD4 and CD8 T cells were present in the granuloma (Figure 1C-ii and -iii), and co-
113 localisation analysis demonstrated that a proportion of both T cell subtypes expressed PD-1
114 (Figure 1C-iv), consistent with the flow cytometry data. In contrast, in caseating granulomas
115 with evident immunopathology, PD-1 expression was totally absent (Figure 1D-i and Figure
116 1–figure supplement 2). The lack of immunoreactivity was not due to lack of viable cells, as
117 CD4 and CD8 expressing T cells were present within the same area (Figure 1D-ii and -iii).
118 Therefore, in human granulomas, PD-1 is expressed in areas where the host-pathogen
119 interaction appears stable but is absent in regions of immunopathology.

120

121 **The PD-1/ PD-L1 axis is up-regulated in the 3D microsphere model**

122 Taken together, these data from Mtb infected patients demonstrate that PD-1 is expressed by
123 lung resident T-cells and may be required to prevent destructive lung disease. However,
124 whether this is a causal associated remains unclear. We therefore explored the biological role
125 of PD-1 expression in a 3-dimensional (3D) human tissue culture model. TB is a human
126 disease characterised by a prolonged host-pathogen interaction in 3D, and is regulated by the

127 extracellular matrix, and previously we have previously developed a 3D cell culture model
128 incorporating extracellular matrix to investigate TB pathogenesis (20, 22). Here, we first
129 studied migration of cells within the alginate-collagen matrix by performing time-lapse
130 microscopy (Figure 2A and Video 1). For this experiment only, UV killed Mtb was used to
131 permit the imaging outside the containment level 3 laboratory. From 24h, progressive
132 accumulation occurs around a central infected core, resulting in a large multicellular
133 granuloma by 48h with dynamic cellular movement similar to the T cell mobility observed in
134 mouse BCG granulomas (23).

135

136 We next investigated whether the PD-1/PD-L1 axis was up-regulated by infection in this 3D
137 model, and found that Mtb infection increased PD-L1 and PD-L2 gene expression at 4 days
138 post infection (Figure 2B). Furthermore, a hypoxic environment (1% oxygen) further
139 increased PD-L2 expression. PD-1 gene expression was not increased at 72h by Mtb infection
140 under normoxic conditions, but was up-regulated when infected cells were incubated in
141 hypoxia (Figure 2B). The change in expression required both infection and hypoxia, as
142 hypoxia did not increase PD-1 or PD-L1/2 expression alone (Figure 2–figure supplement 1).
143 We then studied PD-1/PD-L1 cellular surface expression in microspheres by flow cytometry
144 after one week of infection. Mtb infection slightly increased PD-1 surface expression on
145 CD4⁺ T cells in normoxia, which was augmented by hypoxia (Figure 2C). Similarly, Mtb
146 infection increased PD-1 expression on CD8⁺ T cells, which was greater in hypoxia (Figure
147 2D). Furthermore, on CD14⁺ CD11b⁺ cells, PD-L1 expression was increased by infection and
148 more so in hypoxia (Figure 2E). To investigate whether the effect of hypoxia on increased
149 PD-1/PD-L1 expression was due to altered Mtb growth, we studied proliferation using Mtb
150 expressing firefly luciferase and also colony counting on Middlebrook 7H11 agar. Hypoxia
151 inhibited Mtb growth by both readouts (Figure 2F and Figure 2–figure supplement 2A). As

152 expected, hypoxia also increased expression of the hypoxia inducible factor, HIF-1 α , in host
153 cells (Figure 2G), but did not have a significant effect on host cell survival (Figure 2–figure
154 supplement 2B). Therefore, the increased PD-1 and PD-L1/2 expression in hypoxia was not
155 due to increased Mtb growth or a change in host cell viability.

156

157

158 **PD-1 pathway inhibition increases Mtb growth in the 3D model**

159 Having demonstrated that the PD-1/PD-L1 axis was up-regulated by infection in the 3D
160 model, we investigated whether inhibition of this interaction modulated host control of Mtb.
161 We initially studied chemical inhibitors of the PD-1/PD-L1 axis (Inhibitor 1, C₂₉H₃₃NO₅) and
162 found that blocking PD-1/PD-L1 binding increased Mtb growth in a dose-dependent manner
163 (Figure 3A). This effect occurred in both normoxia and hypoxia (Figure 3–figure supplement
164 1). No effect of PD-1 inhibition on cell survival was noted at day 7 or day 14, utilising two
165 different assays suited to each time point (Figure 3B and C). Next, we studied spartalizumab,
166 a humanised monoclonal antibody with high-affinity to PD-1 that blocks the interaction with
167 PD-L1 and PD-L2 (24). Consistent with the chemical inhibition, PD-1 pathway inhibition
168 using spartalizumab increased Mtb growth in normoxia in a dose-dependent manner (Figure
169 3D). Similarly, in hypoxia spartalizumab increased Mtb growth (Figure 3E). Microspheres
170 must be restored to normoxia to measure Mtb luminescence, and therefore a single time point
171 was analysed. Anti-PD-1 antibody treatment had no significant effect on cell survival in
172 either normoxia or hypoxia (Figure 3F).

173

174

175 **PD-1 inhibition increases secretion of multiple cytokines and growth factors**

176 To investigate the underlying mechanism whereby PD-1 inhibition leads to increased Mtb
177 growth, we studied secretion of cytokines, chemokines and growth factors by measuring
178 accumulation in the media around Mtb-infected microspheres by Luminex array. Mtb
179 infection increased secretion of numerous analytes (Figure 4–figure supplement 1), and
180 inhibition of PD-1/PD-L1 signalling further significantly augmented secretion of twelve
181 analytes compared to Mtb infection alone (Figure 4). A similar augmentation of analyte
182 secretion was observed in hypoxic microspheres (Figure 4–figure supplement 2). The twelve
183 analytes that were further increased above Mtb infection with concurrent PD-1 inhibition
184 were IL-4, IL-6, IL-10, IL-12, TNF- α , IL-1RA, MIP-1 α , MIP-1 β , RANTES, G-CSF, GM-
185 CSF and VEGF (individual concentrations, Figure 4–figure supplement 1). Anti-PD-1 alone
186 increased TNF- α secretion, although to a lesser effect than in combination with Mtb infection
187 (Figure 4–figure supplement 3).

188

189 **Exogenous TNF- α increases Mtb growth in microspheres**

190 To establish which of these factors might be associated with increased Mtb growth, we added
191 the significantly upregulated analytes either individually or in combination pools to 3D
192 microspheres in normoxia at “low” (Figure 5) and “high” concentrations (Figure 5–figure
193 supplement 1), as determined by the concentration measured in the secretion analysis. TNF- α
194 was the dominant cytokine that increased Mtb growth, with other cytokines only having a
195 minor effect (Figure 5A). Chemokines (RANTES, MIP-1 α and MIP-1 β) and growth factors
196 (G-CSF) had no significant effect, while GM-CSF significantly increasing Mtb growth, but
197 the effect was smaller than for TNF- α (Figure 5B). Additionally, the only cytokine
198 combination that had a significant effect on Mtb growth was the pro-inflammatory pool
199 containing TNF- α , IL-6 and IL-12 (Figure 5C). The addition of Th₂ cytokines, chemokines or
200 other growth factors had no significant effect (individual growth curves at “high”

201 concentration, Figure 5–figure supplement 1). Furthermore, TNF- α had a progressive dose-
202 dependent effect increasing Mtb growth within microspheres (Figure 5D).

203

204 To explore the effect of TNF- α further, we then generated microspheres incorporating
205 infected PBMC with and without anti-TNF- α neutralising antibodies. Consistent with our
206 initial observation, anti-TNF- α neutralising antibodies suppressed the TNF-mediated
207 increased Mtb growth, with a partial reduction at each concentration studied of two different
208 neutralising antibodies (Figure 5E and Figure 5–figure supplement 2). Exogenous TNF- α
209 modulated macrophage polarisation within microspheres, reducing CD80 expression at day 7
210 (Figure 5–figure supplement 3). Therefore, we next investigated whether anti-PD-1-induced
211 Mtb growth could be reversed by blocking TNF- α activity. Anti-PD-1 antibody treatment of
212 infected cells again augmented Mtb growth, and this increased growth could be reversed by
213 the incorporation of anti-TNF- α antibodies into the microspheres (Figure 5F). This confirms
214 that an excess of TNF- α is the primary driver of increased Mtb growth caused by PD-1
215 inhibition in the 3D model.

216

217 **TNF- α is highly expressed in TB granulomas and sputum TNF- α negatively correlates**
218 **with circulating PD-1 expression**

219 Finally, to establish the *in vivo* relevance of our cell culture model findings, we performed
220 immunohistochemical analysis of biopsies from patients with standard TB and anti-PD-1
221 associated TB. TNF- α was expressed within TB granulomas, with greater immunoreactivity
222 than control lung tissue at the excision margin of lung cancer (Figure 6A). Consistent with
223 our cell culture observations, TNF- α immunostaining was extensive in a biopsy from a
224 patient that developed pulmonary TB whilst treated with pembrolizumab, an anti-PD-1
225 antibody (Figure 6B). Quantitative analysis of differences between standard TB and anti-PD-

226 1 TB was not possible due to the unique nature of this clinical specimen, as TB diagnosis is
227 usually made by bronchoalveolar lavage as opposed to percutaneous biopsy.

228

229 We then analysed the association between PD-1 expression by circulating CD4⁺ and CD8⁺ T
230 cells and sputum TNF- α concentrations in a previously reported cohort (25). Although this
231 involved comparing PD-1 expression by circulating T cells, remote from the site of disease,
232 with total TNF- α concentration in the sputum, we hypothesised that a reverse association
233 would support the conclusion that PD-1 limits TNF- α secretion in patients. Consistent with
234 this, CD4⁺ T cell PD-1 expression negatively correlated with sputum TNF- α , with a
235 significant negative association despite the relatively low sample numbers, which would be
236 expected to obscure an effect (Figure 6C).

237

238

239

240 **Discussion**

241 Although Mtb kills more people than any other infection worldwide, an enduring enigma is
242 that 90% of those exposed exert lifelong control of the pathogen. In seminal post-mortem
243 studies when TB was highly prevalent in the United States, Opie showed that 30% of humans
244 who died from other causes had viable Mtb present in the lung apices (26). Therefore, in the
245 majority of exposed individuals, a stable relationship forms between host immune cells and
246 Mtb without disease developing. Disseminated TB disease often develops in
247 immunocompromised individuals, such as advanced HIV infection, newborn infants or
248 following anti-TNF- α therapy, and this observation informs the view that TB can arise as a
249 disease of a deficient immune response to the pathogen (3).

250

251 However, the commonest form of human TB, and the one that leads to transmission, is apical
252 pulmonary disease (27). This occurs most frequently in young adults between the ages of 20-
253 25 with the strongest recall response to Mtb antigens, as measured by the Mantoux test (28).
254 Therefore, these clinical observations demonstrate that infection results in a stable symbiosis
255 between host and pathogen in the majority of individuals, and a pronounced immune
256 response associates with the subsequent development of infectious pulmonary disease. The
257 recently emerging clinical phenomenon of TB rapidly developing after initiating anti-PD-1
258 immunotherapy (5-15) further reinforces that an excessive immune response in TB can be
259 harmful.

260

261 PD-1 is expressed on T cells at the site of TB disease and PD-1 expression on circulating
262 CD4⁺ T cells associates with bacterial load (29). PD-1 expression is elevated in circulating
263 CD4 T cells in TB (30) and has been proposed to limit an effective host immune response.
264 Consequently PD-1 inhibition has been advanced as a therapeutic target to accelerate
265 clearance of infection (4, 30-34). However, from an evolutionary perspective, PD-1 is
266 proposed to limit immunopathology in the face of chronic antigenic stimulation (35).
267 Therefore, it is equally plausible, and indeed perhaps more logical, that PD-1/PD-L1 pathway
268 up-regulation in TB is a physiologically appropriate response to the persistent pathogen. We
269 found that hypoxia further up-regulated the PD-1/PD-L1/2 axis, consistent with hypoxia
270 increasing expression in cancer (19), and TB lesions are hypoxic both in model animals and
271 human lesions (18, 36). Analysis of the effect of hypoxia is complicated that both host and
272 pathogen physiology are altered, with hypoxia causing reduced Mtb growth (37-39) but also
273 causing diverse host physiological changes. PD-1 may be particularly important in limiting
274 excessive inflammation and pathology in conditions of low oxygen tension. TB reactivation
275 following immune checkpoint blockade, and the extreme susceptibility of PD-1 deficient

276 mice to Mtb infection (16, 17), would support such a regulatory role, even though it runs
277 counter to widely advanced disease paradigms.

278

279 Our work further highlights the double-edged sword of the host immune response in TB (40).
280 TNF- α is clearly essential to an effective host immune response to TB, as disease frequently
281 develops after treatment with anti-TNF- α antibodies (41), and TNF- α inhibits Mtb growth in
282 zebrafish macrophages (42) and human alveolar macrophages (43). However, excessive
283 TNF- α is also associated with poor outcomes in TB. In human cells, an excess of TNF- α can
284 increase Mtb growth (44, 45), consistent with our observations. In patients with active TB,
285 TNF- α expression by Mtb-specific T cells is increased (46, 47) and TNF- α associates with
286 more severe radiological findings (48, 49). In diverse model systems, excessive TNF- α has
287 been shown to cause harmful inflammation (50-54), consistent with TNF- α exerting a bell-
288 shaped effect on host immunity, with either deficit or excess detrimental. Similarly, we report
289 a deleterious effect of additional GM-CSF, in contrast to GM-CSF improving control of Mtb
290 growth in murine macrophages (55). This suggests that cytokine responses are highly dose
291 and context dependent, potentially with each demonstrated non-linear responses leading to a
292 complex matrix of what may denote the optimal cytokine profile for Mtb control. Consistent
293 with our findings, in the one patient that developed TB on anti-PD-1 treatment where
294 longitudinal samples are available, there was a spike in PPD-specific TNF- α expressing cells
295 prior to with the development of active TB (13), consistent with PD-1 acting as a regulator of
296 TNF- α expression in TB. Taken together, these findings demonstrate a harmful effect of
297 excessive TNF- α in TB.

298

299 We found that multiple cytokines and chemokines were increased after PD-1 inhibition, and
300 therefore events in humans are likely to be more complex than TNF- α excess alone. The
301 augmented inflammation may have multiple harmful effects, such as recruitment of excessive
302 inflammatory cells and destruction of the extracellular matrix (56-58), which favour Mtb
303 growth. In the mouse model of TB, one key role of PD-1 is to limit IFN- γ production (59),
304 and we have shown that excess IFN- γ also accelerates Mtb growth in microspheres (20). We
305 did not show an effect of TNF- α on cell survival, although TNF- α has been reported to
306 increase macrophage necrosis in the zebrafish model, via a mitochondrial-lysosomal-
307 endoplasmic reticulum circuit (53, 60). The effect of PD-1 inhibition on macrophage
308 polarisation and survival warrants further investigation, as this is likely to be one determinant
309 of outcome (61, 62).

310 As in all *in vitro* systems, the bioelectrospray model has limitations (63). For example, it
311 does not permit the ingress of new inflammatory cells, and therefore can only be used to
312 investigate the early events resulting from anti-PD-1 treatment, and not the recruitment of
313 inflammatory cells by increased chemokine secretion. In addition, although it permits longer
314 analysis of the host-pathogen interaction than other human primary cell culture systems, the 3
315 week standard experiment remains shorter than human infection, and so it models early
316 events. We have not yet characterised which cells which produce TNF- α , nor the wider
317 phenotypic changes that result from inhibition of the PD-1 axis. The optimal approach would
318 be to integrate single cell RNAseq to the analysis pipeline, so the phenotype of different cells
319 can be comprehensively analysed. As microspheres can be readily dissolved by incubation in
320 EDTA to release the cells, the system is suited for this technical development.

321

322 The common side effects of anti-PD-1 treatment in patients are termed immune related
323 Adverse Events (irAEs), which are autoimmune in nature (64). We have proposed that an
324 autoimmune process may exacerbate pathology in TB (65), and others have suggested that a
325 loss of tolerance underlies progression to active TB (66, 67). The common theme is that an
326 excessive response to antigens, whether host or pathogen-derived, can drive disease in TB
327 and our findings further support this conclusion. PD-1 may act to fine tune the balance
328 between pro- and anti-inflammatory responses necessary to control infection without causing
329 pathology. Notably, immune related adverse events to immune checkpoint inhibitors may be
330 treated with anti-TNF- α antibodies (64), suggesting TNF- α may be the primary driver of both
331 autoimmunity and TB pathology after PD-1 treatment.

332

333 Our model provides the mechanistic insights into a clinical phenomenon with significant
334 implications for future TB treatment and vaccine approaches. Simply driving a stronger
335 immune response to Mtb seems unlikely to be beneficial, as clinical and epidemiological data
336 suggest it may be harmful. For example, host-directed therapies may be designed to
337 accelerate bacterial clearance whilst concurrently reducing immunopathological effects by
338 appropriate skewing of macrophage phenotype. A more nuanced view considering the
339 different immunological phases of TB is essential, differentiating events at the point of initial
340 exposure from the late events at the apex of the lung, where excessive inflammation leads to
341 immunopathology and transmission (68). Defining the distinction between a protective and
342 pathological immune response in human TB remains a key unanswered question, essential to
343 inform new interventions to control the TB pandemic.

344

345

Key Resources Table				
Reagent type (species) or resource	Designation	Source or reference	Identifiers	Additional information
Strain, strain background (<i>Mycobacterium tuberculosis</i>)	H37Rv	(From Ref: 20)		Used at multiple of infection of 0.1
Strain, strain background (<i>Mycobacterium tuberculosis</i>)	H37Rv pMV306hsp+LuxAB+G13+CD E	(From Ref: 20)		Used at multiple of infection of 0.1
Strain, strain background (<i>Mycobacterium tuberculosis</i>)	H37Rv pMV306hsp encoding the wild-type FFluc	(From Ref: 20)		Used at multiple of infection of 0.1
Biological sample (Antibodies)				
Antibody	anti-CD45-V500 Horizon (Clone no. HI30)	BD Biosciences	Cat.No.563792	Monoclonal mouse antibody
Antibody	anti-CD3 Brilliant Violet 785 (Clone no. OKT3)	Biolegend	Cat.No.317330	Monoclonal mouse antibody
Antibody	anti-CD3-PE (Clone no. HIT3a)	Biolegend	Cat.No.300308	Monoclonal mouse antibody
Antibody	anti-CD4 Brilliant Ultra Violet 496 (Clone no. SK3)	BD Bioscience	Cat.No.612937	Monoclonal mouse antibody
Antibody	anti-CD4-PerCP (Clone no. OKT4)	Biolegend	Cat.No.317432	Monoclonal mouse antibody
Antibody	anti-CD8 Brilliant Violet 605 (Clone no. RPA-T8)	Biolegend	Cat.No.301040	Monoclonal mouse antibody
Antibody	anti-CD8-APC (Clone no. SK1)	Biolegend	Cat.No.344722	Monoclonal mouse antibody
Antibody	anti-CD103-APC (Clone no. Ber-ACT8)	BD Biosciences	Cat.No.563883	Monoclonal mouse antibody
Antibody	anti-CD69 Brilliant Ultra Violet 395 (Clone no. FN50)	Biolegend	Cat.No.310902	Monoclonal mouse antibody
Antibody	anti-HLA-DR-PerCP (Clone no. L243)	Biolegend	Cat.No.307628	Monoclonal mouse antibody
Antibody	anti-CD279-BB515 (Clone no. EH12.1)	BD Biosciences	Cat.No.564494	Monoclonal mouse antibody
Antibody	anti- CD-274-BB515 (Clone no. MIH1)	BD Biosciences	Cat.No.564554	Monoclonal mouse antibody
Antibody	anti-PD-1 Brilliant Violet 421 (Clone no.EH12.1)	BD Biosciences	Cat.No.562516	Monoclonal mouse antibody
Antibody	anti-CD11b-APC (Clone no. ICRF44)	Biolegend	Cat.No.301310	Monoclonal mouse antibody
Antibody	anti-CD45-APC/Cy7 (Clone no. 2D1)	Biolegend	Cat.No.368516	Monoclonal mouse antibody
Antibody	anti-CD14-AP/APC (Clone no. HCD14)	Biolegend	Cat.No.325608	Monoclonal mouse antibody
Antibody	anti-True-Stain Monocyte Blocker™	Biolegend	Cat.No.426102	Monoclonal mouse antibody
Antibody	anti-CD4 (Clone no. M7310)	DAKO	Cat.No.M7310	Monoclonal mouse antibody

Antibody	anti-CD8 (Clone no. M7103)	DAKO	Cat.No. M7103	Monoclonal mouse antibody
Antibody	anti-PD1 (Clone no. ab5287)	Abcam	Cat.No.ab52587	Monoclonal mouse antibody
Antibody	anti-TNF- α (Clone no. ab1793)	Abcam	Cat.No.ab1793	Monoclonal mouse antibody
Antibody	Spartalizumab	Selleckchem	Cat.No.A2017	20 μ g/ml and 200 μ g/ml, monoclonal, mouse IgG4
Antibody	IgG4	Sino Biologicals	Cat.No.13505-HNAH	20 μ g/ml and 200 μ g/ml, monoclonal, mouse IgG4
Antibody	Mouse IgG1 kappa Isotype Control (P3.6.2.8.1),	Thermo Fisher Scientific	Cat.No.16-4714-82	50 μ g/ml, mouse monoclonal IgG2A
Antibody	Mouse IgG1 Negative Control, clone Ci4	Merck Life Sciences	Cat.No.MABC002	51 μ g/ml, mouse monoclonal IgG2A
Antibody	anti-TNF- α	Thermo Fisher Scientific	Cat.No.16-7348-81	52 μ g/ml, mouse monoclonal IgG2A
Sequence-based reagent (Applied Biosystems TaqMan Gene Expression primers)	GAPDH	Thermo Fisher Scientific	#Hs02758991_g1	
	β 2-Microbulin	Thermo Fisher Scientific	#Hs00608023_m1	
	FNTA	Thermo Fisher Scientific	#Hs00357739_m1	
	PDCD1	Thermo Fisher Scientific	#Hs01550088_m1	
	CD274	Thermo Fisher Scientific	#Hs00204257_m1	
	PDCD1LG2	Thermo Fisher Scientific	#Hs00228839_m1	
	HIF-1 α	Thermo Fisher Scientific	#Hs00153153_m1	
Commercial assay or kit	CytoTox-Glo Cytotoxicity Assay	Promega	G9291	Commercial assay or kit
	Lactate Dehydrogenase Activity Assay Kit	Merck	11 644 793 001	Commercial assay or kit
	Cytokine and Chemokine 35-Plex Human ProcartaPlex™ Panel	Thermo Fisher Scientific	LHC6005M	Commercial assay or kit
Chemical compound, drug	PD-1/PD-L1 Inhibitor 1	Cambridge Biosciences, UK	#1675201-83-8	Chemical compound
	Recombinant Human G-CSF	ImmunoTools	Cat.No.11343115	1 ng/ml and 5 ng/ml

	Recombinant Human GM-CSF	ImmunoTools	Cat.No.11343125	0.25 ng/ml and 1.25 ng/ml
	Recombinant Human IL-1RA / IL1F3	ImmunoTools	Cat.No.11344876	1.25 ng/ml and 6.25 ng/ml
	Recombinant Human IL-10	ImmunoTools	Cat.No.11340105	0.2 ng/ml and 1 ng/ml
	Recombinant Human IL-6	ImmunoTools	Cat.No.11340066	10.0 ng/ml and 50.0 ng/ml
	Recombinant Human IL-12	ImmunoTools	Cat.No.11349125	0.5 ng/ml and 2.5 ng/ml
	Recombinant Human TNF- α	ImmunoTools	Cat.No.11343017	0.3 ng/ml , 1.5 ng/ml, 7.5ng/ml and 15ng/ml
	Recombinant Human IL-15	ImmunoTools	Cat.No.11340155	0.5ng/ml, 5ng/ml and 50ng/ml
	Recombinant Human IL-17A	ImmunoTools	Cat.No.11340176	1 ng/ml , 10ng/ml and 100ng/ml
	Recombinant Human IL-17F	ImmunoTools	Cat.No.11349176	1 ng/ml , 10ng/ml and 100ng/ml
	Recombinant Human RANTES	ImmunoTools	Cat.No.11343196	0.3 ng/ml and 1.5 ng/ml
	Recombinant Human MIP-1 α	ImmunoTools	Cat.No.11343206	1.5 ng/ml and 7.5 ng/ml
	Recombinant Human MIP-1 β	ImmunoTools	Cat.No.11343223	1.0 ng/ml and 5 ng/ml
	Recombinant Human MCP	ImmunoTools	Cat.No.11343386	1 ng/ml , 10ng/ml and 100ng/ml
Software, algorithm	FlowJo	BD Biosciences	version 10.6.1	Software
	BD FACSDiva™ Software	BD Biosciences		Software
	Graphpad Prism	GraphPad Software LLC	v7.05	Software

347

348 ***M. tuberculosis* culture**

349 *M. tuberculosis* H37Rv (Mtb) was cultured in Middlebrook 7H9 medium (supplemented with
350 10% ADC, 0.2% glycerol and 0.02% Tween 80) (BD Biosciences, Oxford). Bioluminescent
351 Mtb containing luxABCDE (Mtb lux+) and Mtb expressing ffLuc (Mtb ffLuc+) were
352 cultured with kanamycin 25µg/ml. Luminescence was measured with either GloMax® 20/20
353 single tube luminometer (Promega,UK) or GloMax® Discover microplate reader
354 (Promega,UK). Cultures at 1×10^8 CFU/ml Mtb (OD= 0.6) were used for all experiments at
355 multiplicity of infection (MOI) of 0.1. Live Mtb was used in all experiments apart from the
356 time lapse microscopy, which used UV killed TB. Mtb colony counting was performed by
357 serial dilution on Middlebrook 7H11 Agar. Bioluminescence from the Mtb ffLuc+ was
358 induced using D-luciferin (ThermoFisher, UK) at a concentration of 750µM in Hank's
359 balanced salt solution (HBSS).

360 **PBMC cell isolation from human blood**

361 For the 3D microsphere experiments, PBMC were separated from single donor leukocyte
362 cones (National Health Service Blood and Transfusion, Southampton, UK) by density
363 gradient centrifugation over Ficoll-Paque (GE Healthcare Life Sciences). Ethical approval for
364 these studies was provided by the National Research Ethics Service Committee South Central
365 - Southampton A, ref 13/SC/0043.

366 Study participants for the correlation analysis of sputum-TNF- α with PD-1 expression on
367 CD4⁺ and CD8⁺ T cells are the cross-sectional study individuals in a previously reported
368 cohort (25, 69). Participants were recruited from an outpatient clinic in Khayelitsha, South
369 Africa and were either healthy volunteers, non-TB respiratory symptomatics or recently
370 diagnosed TB patients. Flow cytometric analysis was performed on cryopreserved PBMC
371 isolated from whole blood as previously reported (69). The study was approved by the

372 University of Cape Town Human Research Ethics Committee (REF 516/2011) and conducted
373 in accordance with the Declaration of Helsinki.

374 **Analysis of PD-1 expression in blood and lung of TB patients**

375 Lung tissue and matched PBMC were obtained from the AHRI Lung study cohort approved
376 by the Biomedical Research Ethics Committee (BREC) of the University of Kwa-Zulu Natal,
377 BREC reference: BE019/13. All participants underwent surgical resection to treat TB related
378 lung complications, including haemoptysis, bronchiectasis, persistent cavitary disease,
379 shrunken or collapsed lung or drug-resistant infection, at the King Dinuzulu Hospital in
380 Durban, KwaZulu- Natal and Inkosi Albert Luthuli Central Hospital (IALCH) in Durban,
381 KwaZulu-Natal. PBMC were isolated from whole blood using standard Ficoll-Histopaque
382 (Sigma) density gradient centrifugation by standard protocol.

383 Lung tissues was cut into approximately 1mm³ pieces, washed several times with cold HBSS
384 (Lonza) and re-suspended in 8mls of pre-warmed digestion media R10 (RPMI supplemented
385 with 10% FCS, 2 mM L-glutamate, 100 U/ml Penstrep), containing 0.5 mg/ml collagenase D
386 (Roche) and 40 U/ml DNaseI (Roche), and transferred to GentleMACS C-tubes (Miltenyi)
387 for mechanical digestion according to the manufacturer's instructions. The suspension was
388 incubated for 30 minutes at 37° C, followed by an additional mechanical digestion step and
389 another 30-minute incubation step at 37°C. The final suspension was passed through a 70 µm
390 cell strainer and washed twice in HBSS. PBMC and lung cells were phenotyped by surface
391 staining with a near-infrared live/dead cell viability cell staining kit (Invitrogen) and a
392 cocktail of fluorochrome conjugated antibodies: αCD45-V500 Horizon clone HI30 (BD
393 Biosciences), αCD3 Brilliant Violet 785 clone OKT3 (Biolegend), αCD4 Brilliant Ultra
394 Violet 496 clone SK3 (BD Bioscience), αCD8 Brilliant Violet 605 clone RPA-T8
395 (Biolegend), αCD103-APC clone Ber-ACT8 (BD Biosciences), αCD69 Brilliant Ultra Violet

396 395 clone FN50 (Brilliant Horizon), α PD-1 Brilliant Violet 421 clone EH12.1 (BD
397 Biosciences). Cells were stained with 25uL of antibody cocktail in the dark for 20 minutes at
398 room temperature followed by washing with PBS, then fixed in 2% PFA. Data was acquired
399 using BD Aria Fusion cytometer and analyzed using FlowJo Software v.9.9 (Treestar Inc,
400 Ashland, OR).

401 **Immunohistochemistry of paraffin-fixed tissue**

402 Immunohistochemical analysis was performed on paraffin-embedded lung tissue from
403 patients with pulmonary TB and lung cancer that were mounted at 4 μ m thin onto APS coated
404 glass slides and dried, using the following antibodies: anti-CD4 (Clone no. M7310) (DAKO),
405 anti-CD8 (Clone no. M7103) (DAKO), anti-PD1 (Clone no. ab5287) (Abcam) and anti-TNF-
406 α (Clone no. ab1793) (Abcam). Staining was done at optimised concentrations
407 using recommended buffers for each antibody.

408 **Microencapsulation of cells**

409 Microspheres were generated with an electrostatic generator (Nisco, Zurich, Switzerland) as
410 described previously (1). Briefly, PBMC were infected overnight with Mtb in a 250cm² flask,
411 cells were detached, pelleted and mixed with 1.5% sterile alginate (Pronova UP MVG
412 alginate, Nova Matrix, Norway) and 1mg/mL collagen (Advanced BioMatrix, USA) at a final
413 concentration of 5 x 10⁶ cells/ml. The cell-alginate suspension was injected into the bead
414 generator where microspheres were formed in an ionotropic gelling bath of 100mM CaCl₂ in
415 HBSS. After washing twice with HBSS with Ca²⁺/Mg²⁺, microspheres were transferred in
416 RPMI 1640 medium containing 10% human AB serum and incubated at 37°C. Microspheres
417 were either dispensed into eppendorfs, which were then randomly allocated to different
418 environmental conditions, or plated into a 96-well plate with conditions in triplicate
419 according to a pre-determined template. For experiments in hypoxia, microspheres were

420 incubated in 1% oxygen in Galaxy 48 R CO₂ incubator (Eppendorf, UK) until analysis.
421 Supernatants were collected at defined time points. Time points described are days post
422 infection.

423 **Live Cell Imaging**

424 Uninfected or UV killed Mtb infected cells suspended in alginate-collagen matrix were plated
425 in an 8 well μ -Slide (ibidi GmbH, Germany). HBSS containing Ca²⁺ was used for cross-
426 linking of alginate in the extracellular matrix for 15 minutes and then replaced with RPMI
427 medium with 10% human AB serum. Samples were imaged using an Olympus IX81 time-
428 lapse microscope with temperature of 37°C and CO₂ concentration 5%. Z-stacks 200 μ m in
429 height were captured at one position in each sample every 30 minutes for 48 hours. Images
430 were exported as tif files and opened in ImageJ.

431 **PD-1/PD-L1 Inhibition**

432 Small chemical inhibition of PD-1/PD-L1 signalling was by PD-1/PD-L1 Inhibitor 1 (CAS
433 Registry #1675201-83-8, Cambridge Biosciences, UK), a compound that competitively
434 blocks the interaction of PD-1 with its ligand protein PD-L1 (70). Inhibitor 1 was prepared in
435 DMSO (Sigma-Aldrich, UK) at a concentration of 6.3mM and dissolved to a concentration of
436 1nM, 10nM, 100nM and 1 μ M in complete media and added to media around microspheres on
437 the day after encapsulation. Luminescence was monitored on specific days. For the
438 microspheres incubated in hypoxic conditions, measurement of luminescence was repeated
439 for every 30 minutes after the addition of luciferin until the reading plateaued, which was
440 usually 2 hrs.

441 In antibody inhibitory experiments, spartalizumab (Selleckchem, Germany), a humanised
442 IgG4 anti-PD1 monoclonal antibody, was used to inhibit of PD-1/PD-L1 signalling in
443 microspheres. Briefly, cells were infected with Mtb overnight, pelleted and then a suspension

444 of anti-PD1 antibodies (20 and 200 μ g/ml) were added and pre-incubated for 1 hour. Cells
445 were then encapsulated within microspheres and kept for 14 days in either normoxia or 1%
446 oxygen at 37°C and 5% CO₂. Mtb growth was measured using luminescence and
447 supernatants were taken for either cytokine or LDH measurement. An IgG4 human antibody
448 was used at the same concentration as a control.

449 **Cell Toxicity Assays**

450 Lactate dehydrogenase (LDH) release in the supernatants collected at different time points
451 was analysed by a colorimetric activity assay as per manufacturer's instructions (Roche,
452 Burgess Hill, United Kingdom). As a second assay, CytoTox-Glo Cytotoxicity Assay
453 (Promega) was used, which measures dead-cell protease activity released from cells without
454 membrane integrity using a luminogenic peptide substrate, the AAF-Glo™ Substrate.
455 Luminescence from 96-well plates was analysed by GloMax Discover (Promega). The LDH
456 assay was suited for later time points, as this could be performed on microspheres in
457 eppendorfs, while the CytoTox glow required analysis in 96 well plates and so was best
458 suited to analysis in the first week.

459 **Gene Expression Analysis**

460 All the reagents were sourced from ThermoFisher Scientific (Paisley, UK). In brief,
461 microspheres were decapsulated with 5mM EDTA, cells were pelleted and immediately lysed
462 using TRIzol Reagent. RNA was transcribed using High Capacity cDNA Reverse
463 Transcription kit. TaqMan® Universal master mix and primers specific for genes were
464 GAPDH (#Hs02758991_g1), β 2-Microbulin (#Hs00608023_m1), FNTA
465 (#Hs00357739_m1), PDCD1 (#Hs01550088_m1), CD274 (#Hs00204257_m1), PDCD1LG2
466 (#Hs00228839_m1) and HIF-1 α (Hs00153153_m1) were used for qPCR according to the

467 manufacturer's instructions and the comparative threshold (CT) method was employed to
468 analyse all qPCR data.

469 **Immunophenotyping of cells from microspheres**

470 Microspheres were decapsulated with 5mM EDTA in HBSS with no $\text{Ca}^{2+}/\text{Mg}^{2+}$ at day 7 after
471 encapsulation and 2 million cells prepared for staining in RPMI with 5% foetal bovine serum.
472 To measure the expression of PD-1 in CD4^+ and CD8^+ T cells and PD-L1 expression in
473 $\text{CD14}^+\text{CD11b}^+$ cells, the following antibody panel was used: CD3-PE (clone HIT3a,
474 Biolegend), HLA-DR-PerCP (clone L243, Biolegend), CD4-PerCP (clone OKT4,
475 Biolegend), CD8-APC (clone SK1, Biolegend), CD11b-APC (clone ICRF44, Biolegend),
476 CD45-APC/Cy7 (clone 2D1, Biolegend), CD14-AP/APC (clone HCD14, Biolegend),
477 CD279-BB515 (Clone EH12.1, BD), CD-274-BB515 (Clone MIH1, BD) and True-Stain
478 Monocyte Blocker™ (Biolegend, USA). Gates were defined using fluorescence minus one
479 control after exclusion of the dead cells using Live/Dead fixable stain (ThermoFisher, UK).
480 Gating strategy is provided in Figure 5–figure supplement 4. Cells were acquired after fixing
481 them in 2% paraformaldehyde in HBSS for 1 hour using FACSAria (Becton Dickinson, UK)
482 and analysed by FACSDiva software (Becton Dickinson) and Flow Jo version 10 (Treestar).

483 **Cytokine supplementation**

484 Microspheres were incubated in RPMI 1640 with 10% AB serum in an opaque 12-well tissue
485 culture plate with G-CSF, GM-CSF, IL-1RA, IL-6, IL-10, IL-12, IL-15, IL-17A, IL-17F,
486 TNF- α , RANTES, MIP-1 α , MIP-1 β and MCP at two concentrations determined by the
487 cellular experiments, at 37°C and 5% CO_2 . All the cytokines were purchased from
488 ImmunoTools (Germany), suspended in RPMI with 0.1% human serum and kept at -80°C
489 until use. Bacterial growth was monitored with luminescence using GloMax® Discover
490 microplate reader (Promega,UK).

491 **Luminex Analysis**

492 Samples were sterilised by filtration through a 0.22 μ M Durapore membrane (MerkMillipore).
493 Concentrations of cytokines (ThermoFisher, UK) were determined using a Bioplex 200
494 platform (Bio-Rad, UK) according to the manufacturer's protocol and quantified per
495 milligram of total protein measured by Bradford assay (Biorad).

496 **Statistical analysis**

497 All experiments were performed on a minimum of 2 occasions from separate donors as
498 biological replicates and on each occasion with a minimum of 3 technical replicates. Some
499 donor-to-donor variation occurred in terms of absolute RLU, as expected in the analysis of
500 primary human cells, but the direction of effects were always consistent. Data presented are
501 from a representative donor and include the mean and SEM. Analysis was performed in
502 Graphpad Prism v7.05. Students t-test was used to compare pairs and ANOVA with Tukey's
503 correction for multiple comparisons for groups of 3 or more groups where it was appropriate.
504 For the flow cytometric analysis of clinical samples, data were analysed using Mann-Whitney
505 test for comparing pairs and Kruskal-Wallis test with Dunn's multiple comparisons test for 3
506 or more group.

507 **Acknowledgements**

508 This work was supported by the UK Medical Research Council MR/N006631/1 (PE), an
509 Innovation Grant 2017 from Wessex Medical Research and a Postdoctoral Career Track
510 Award from University of Southampton (LT). AL was supported by BMGF (OPP1137006)
511 and the Wellcome Trust (210662/Z/18/Z). SM was supported by Cancer Research UK
512 (23562) and UK Medical Research Council (MR/S024220/1). RJW and KAW receive
513 support from the Francis Crick Institute, which is funded Wellcome Trust (FC0010218), UK
514 research and Innovation (FC0010218), and Cancer Research UK (FC0010218). RJW also
515 receives support from Wellcome Trust (203135, 104803) and NIH, USA (U19AI111276).
516 NFW was supported by an NIHR Academic Clinical Lectureship. We also thank the
517 Department of Infection Biology at London School of Hygiene and Tropical Medicine for
518 access to facilities. We thank Jennifer Russell, Regina Teo and Monette Lopez, University of
519 Southampton, for excellent technical assistance. We thank Siouxsie Wiles for providing the
520 Lux-expressing Mtb.

521

522

523

524 **References**

525

- 526 1. Wallis RS, Maeurer M, Mwaba P, Chakaya J, Rustomjee R, Migliori GB, et al. Tuberculosis-
527 advances in development of new drugs, treatment regimens, host-directed therapies, and biomarkers.
528 *Lancet Infect Dis.* 2016;16(4):e34-46.
- 529 2. Menardo F, Duchêne S, Brites D, Gagneux S. The molecular clock of *Mycobacterium*
530 tuberculosis. *PLoS pathogens.* 2019;15(9):e1008067.
- 531 3. O'Garra A, Redford PS, McNab FW, Bloom CI, Wilkinson RJ, Berry MP. The immune
532 response in tuberculosis. *Annu Rev Immunol.* 2013;31:475-527.
- 533 4. Zumla A, Rao M, Wallis RS, Kaufmann SH, Rustomjee R, Mwaba P, et al. Host-directed
534 therapies for infectious diseases: current status, recent progress, and future prospects. *Lancet Infect*
535 *Dis.* 2016;16(4):e47-63.
- 536 5. Fujita K, Terashima T, Mio T. Anti-PD1 Antibody Treatment and the Development of Acute
537 Pulmonary Tuberculosis. *J Thorac Oncol.* 2016;11(12):2238-40.
- 538 6. Lee JJ, Chan A, Tang T. Tuberculosis reactivation in a patient receiving anti-programmed
539 death-1 (PD-1) inhibitor for relapsed Hodgkin's lymphoma. *Acta Oncol.* 2016;55(4):519-20.
- 540 7. Chu YC, Fang KC, Chen HC, Yeh YC, Tseng CE, Chou TY, et al. Pericardial Tamponade
541 Caused by a Hypersensitivity Response to Tuberculosis Reactivation after Anti-PD-1 Treatment in a
542 Patient with Advanced Pulmonary Adenocarcinoma. *J Thorac Oncol.* 2017;12(8):e111-e4.
- 543 8. Picchi H, Mateus C, Chouaid C, Besse B, Marabelle A, Michot JM, et al. Infectious
544 complications associated with the use of immune checkpoint inhibitors in oncology: reactivation of
545 tuberculosis after anti PD-1 treatment. *Clinical Microbiology and Infection.* 2018;24(3):216-8.
- 546 9. Jensen KH, Persson G, Bondgaard AL, Pohl M. Development of pulmonary tuberculosis
547 following treatment with anti-PD-1 for non-small cell lung cancer. *Acta Oncol.* 2018;57(8):1-2.
- 548 10. Elkington PT, Bateman AC, Thomas GJ, Ottensmeier CH. Implications of Tuberculosis
549 Reactivation after Immune Checkpoint Inhibition. *Am J Respir Crit Care Med.* 2018;198(11):1451-3.

- 550 11. He W, Zhang X, Li W, Kong C, Wang Y, Zhu L, et al. Activated pulmonary tuberculosis in a
551 patient with melanoma during PD-1 inhibition: a case report. *Onco Targets Ther.* 2018;11:7423-7.
- 552 12. Takata S, Koh G, Han Y, Yoshida H, Shiroyama T, Takada H, et al. Paradoxical response in a
553 patient with non-small cell lung cancer who received nivolumab followed by anti-Myco**ba**cterium
554 tuberculosis agents. *J Infect Chemother.* 2019;25(1):54-8.
- 555 13. Barber DL, Sakai S, Kudchadkar RR, Fling SP, Day TA, Vergara JA, et al. Tuberculosis
556 following PD-1 blockade for cancer immunotherapy. *Sci Transl Med.* 2019;11(475).
- 557 14. Tsai CC, Chen JH, Wang YC, Chang FY. Re-activation of pulmonary tuberculosis during
558 anti-programmed death-1 (PD-1) treatment. *QJM.* 2019;112(1):41-2.
- 559 15. van Eeden R, Rapoport BL, Smit T, Anderson R. Tuberculosis Infection in a Patient Treated
560 With Nivolumab for Non-small Cell Lung Cancer: Case Report and Literature Review. *Front Oncol.*
561 2019;9:659.
- 562 16. Lazar-Molnar E, Chen B, Sweeney KA, Wang EJ, Liu W, Lin J, et al. Programmed death-1
563 (PD-1)-deficient mice are extraordinarily sensitive to tuberculosis. *Proc Natl Acad Sci U S A.*
564 2010;107(30):13402-7.
- 565 17. Barber DL, Mayer-Barber KD, Feng CG, Sharpe AH, Sher A. CD4 T cells promote rather
566 than control tuberculosis in the absence of PD-1-mediated inhibition. *J Immunol.* 2011;186(3):1598-
567 607.
- 568 18. Belton M, Brilha S, Manavaki R, Mauri F, Nijran K, Hong YT, et al. Hypoxia and tissue
569 destruction in pulmonary TB. *Thorax.* 2016;71(12):1145-53.
- 570 19. Noman MZ, Desantis G, Janji B, Hasmim M, Karray S, Dessen P, et al. PD-L1 is a novel
571 direct target of HIF-1alpha, and its blockade under hypoxia enhanced MDSC-mediated T cell
572 activation. *J Exp Med.* 2014;211(5):781-90.
- 573 20. Tezera LB, Bielecka MK, Chancellor A, Reichmann MT, Shammari BA, Brace P, et al.
574 Dissection of the host-pathogen interaction in human tuberculosis using a bioengineered 3-
575 dimensional model. *eLife.* 2017;6:e21283.

- 576 21. Snyder ME, Finlayson MO, Connors TJ, Dogra P, Senda T, Bush E, et al. Generation and
577 persistence of human tissue-resident memory T cells in lung transplantation. *Science Immunology*.
578 2019;4(33):eaav5581.
- 579 22. Tezera LB, Bielecka MK, Elkington PT. Bioelectrospray Methodology for Dissection of the
580 Host-pathogen Interaction in Human Tuberculosis. *Bio Protoc*. 2017;7(14).
- 581 23. Egen JG, Rothfuchs AG, Feng CG, Winter N, Sher A, Germain RN. Macrophage and T Cell
582 Dynamics during the Development and Disintegration of Mycobacterial Granulomas. *Immunity*.
583 2008;28(2):271-84.
- 584 24. Kaplon H, Reichert JM. Antibodies to watch in 2019. *mAbs*. 2019;11(2):219-38.
- 585 25. Walker NF, Wilkinson KA, Meintjes G, Tezera LB, Goliath R, Peyper JM, et al. Matrix
586 Degradation in Human Immunodeficiency Virus Type 1-Associated Tuberculosis and Tuberculosis
587 Immune Reconstitution Inflammatory Syndrome: A Prospective Observational Study. *Clin Infect Dis*.
588 2017;65(1):121-32.
- 589 26. Opie EL, Aronson JD. Tubercle bacilli in latent tuberculous lesions and in lung tissue without
590 tuberculous lesions. *Arch Pathol Lab Med*. 1927;4(1):1-21.
- 591 27. Elkington PT, D'Armiento JM, Friedland JS. Tuberculosis immunopathology: the neglected
592 role of extracellular matrix destruction. *Sci Transl Med*. 2011;3(71):71ps6.
- 593 28. Comstock GW, Livesay VT, Woolpert SF. The prognosis of a positive tuberculin reaction in
594 childhood and adolescence. *American journal of epidemiology*. 1974;99(2):131-8.
- 595 29. Day CL, Abrahams DA, Bunjun R, Stone L, de Kock M, Walzl G, et al. PD-1 Expression on
596 Mycobacterium tuberculosis-Specific CD4 T Cells Is Associated With Bacterial Load in Human
597 Tuberculosis. *Frontiers in immunology*. 2018;9:1995.
- 598 30. Shen L, Gao Y, Liu Y, Zhang B, Liu Q, Wu J, et al. PD-1/PD-L pathway inhibits M.tb-
599 specific CD4(+) T-cell functions and phagocytosis of macrophages in active tuberculosis. *Sci Rep*.
600 2016;6:38362.
- 601 31. Jurado JO, Alvarez IB, Pasquinelli V, Martinez GJ, Quiroga MF, Abbate E, et al.
602 Programmed death (PD)-1:PD-ligand 1/PD-ligand 2 pathway inhibits T cell effector functions during
603 human tuberculosis. *J Immunol*. 2008;181(1):116-25.

- 604 32. Singh A, Mohan A, Dey AB, Mitra DK. Inhibiting the programmed death 1 pathway rescues
605 Mycobacterium tuberculosis-specific interferon gamma-producing T cells from apoptosis in patients
606 with pulmonary tuberculosis. *J Infect Dis.* 2013;208(4):603-15.
- 607 33. Suarez GV, Melucci Ganzarain CDC, Vecchione MB, Trifone CA, Marin Franco JL, Genoula
608 M, et al. PD-1/PD-L1 Pathway Modulates Macrophage Susceptibility to Mycobacterium tuberculosis
609 Specific CD8(+) T cell Induced Death. *Sci Rep.* 2019;9(1):187.
- 610 34. Jiang J, Wang X, An H, Yang B, Cao Z, Liu Y, et al. Mucosal-associated invariant T-cell
611 function is modulated by programmed death-1 signaling in patients with active tuberculosis. *Am J*
612 *Respir Crit Care Med.* 2014;190(3):329-39.
- 613 35. Sharpe AH, Pauken KE. The diverse functions of the PD1 inhibitory pathway. *Nat Rev*
614 *Immunol.* 2018;18(3):153-67.
- 615 36. Via LE, Lin PL, Ray SM, Carrillo J, Allen SS, Eum SY, et al. Tuberculous granulomas are
616 hypoxic in guinea pigs, rabbits, and nonhuman primates. *Infect Immun.* 2008;76(6):2333-40.
- 617 37. Devasundaram S, Gopalan A, Das SD, Raja A. Proteomics Analysis of Three Different
618 Strains of Mycobacterium tuberculosis under In vitro Hypoxia and Evaluation of Hypoxia Associated
619 Antigen's Specific Memory T Cells in Healthy Household Contacts. *Frontiers in microbiology.*
620 2016;7:1275-.
- 621 38. Ortega C, Liao R, Anderson LN, Rustad T, Ollodart AR, Wright AT, et al. Mycobacterium
622 tuberculosis Ser/Thr Protein Kinase B Mediates an Oxygen-Dependent Replication Switch. *PLOS*
623 *Biology.* 2014;12(1):e1001746.
- 624 39. Eoh H, Rhee KY. Multifunctional essentiality of succinate metabolism in adaptation to
625 hypoxia in *Mycobacterium tuberculosis*. *Proceedings of the National Academy*
626 *of Sciences.* 2013;110(16):6554.
- 627 40. Ehlers S. Immunity to tuberculosis: a delicate balance between protection and pathology.
628 *FEMS Immunol Med Microbiol.* 1999;23(2):149-58.
- 629 41. Keane J, Gershon S, Wise RP, Mirabile-Levens E, Kasznica J, Schwieterman WD, et al.
630 Tuberculosis associated with infliximab, a tumor necrosis factor alpha-neutralizing agent. *N Engl J*
631 *Med.* 2001;345(15):1098-104.

- 632 42. Clay H, Volkman HE, Ramakrishnan L. Tumor necrosis factor signaling mediates resistance
633 to mycobacteria by inhibiting bacterial growth and macrophage death. *Immunity*. 2008;29(2):283-94.
- 634 43. Hirsch CS, Ellner JJ, Russell DG, Rich EA. Complement receptor-mediated uptake and tumor
635 necrosis factor-alpha-mediated growth inhibition of *Mycobacterium tuberculosis* by human alveolar
636 macrophages. *The Journal of Immunology*. 1994;152(2):743.
- 637 44. Byrd TF. Tumor necrosis factor alpha (TNFalpha) promotes growth of virulent
638 *Mycobacterium tuberculosis* in human monocytes iron-mediated growth suppression is correlated
639 with decreased release of TNFalpha from iron-treated infected monocytes. *J Clin Invest*.
640 1997;99(10):2518-29.
- 641 45. Engele M, Stossel E, Castiglione K, Schwerdtner N, Wagner M, Bolcskei P, et al. Induction
642 of TNF in human alveolar macrophages as a potential evasion mechanism of virulent *Mycobacterium*
643 *tuberculosis*. *J Immunol*. 2002;168(3):1328-37.
- 644 46. Harari A, Rozot V, Enders FB, Perreau M, Stalder JM, Nicod LP, et al. Dominant TNF-
645 alpha+ *Mycobacterium tuberculosis*-specific CD4+ T cell responses discriminate between latent
646 infection and active disease. *Nat Med*. 2011;17(3):372-6.
- 647 47. Tebruegge M, Dutta B, Donath S, Ritz N, Forbes B, Camacho-Badilla K, et al. *Mycobacteria*-
648 Specific Cytokine Responses Detect Tuberculosis Infection and Distinguish Latent from Active
649 Tuberculosis. *Am J Respir Crit Care Med*. 2015;192(4):485-99.
- 650 48. Casarini M, Ameglio F, Alemanno L, Zangrilli P, Mattia P, Paone G, et al. Cytokine levels
651 correlate with a radiologic score in active pulmonary tuberculosis. *Am J Respir Crit Care Med*.
652 1999;159(1):143-8.
- 653 49. Tsao TC, Hong J, Li LF, Hsieh MJ, Liao SK, Chang KS. Imbalances between tumor necrosis
654 factor-alpha and its soluble receptor forms, and interleukin-1beta and interleukin-1 receptor antagonist
655 in BAL fluid of cavitary pulmonary tuberculosis. *Chest*. 2000;117(1):103-9.
- 656 50. Bekker LG, Moreira AL, Bergtold A, Freeman S, Ryffel B, Kaplan G. Immunopathologic
657 effects of tumor necrosis factor alpha in murine mycobacterial infection are dose dependent. *Infect*
658 *Immun*. 2000;68(12):6954-61.

- 659 51. Taylor JL, Ordway DJ, Troudt J, Gonzalez-Juarrero M, Basaraba RJ, Orme IM. Factors
660 associated with severe granulomatous pneumonia in Mycobacterium tuberculosis-infected mice
661 vaccinated therapeutically with hsp65 DNA. *Infect Immun.* 2005;73(8):5189-93.
- 662 52. Tsenova L, Bergtold A, Freedman VH, Young RA, Kaplan G. Tumor necrosis factor alpha is
663 a determinant of pathogenesis and disease progression in mycobacterial infection in the central
664 nervous system. *Proc Natl Acad Sci U S A.* 1999;96(10):5657-62.
- 665 53. Roca FJ, Ramakrishnan L. TNF dually mediates resistance and susceptibility to mycobacteria
666 via mitochondrial reactive oxygen species. *Cell.* 2013;153(3):521-34.
- 667 54. Tzelepis F, Blagih J, Khan N, Gillard J, Mendonca L, Roy DG, et al. Mitochondrial
668 cyclophilin D regulates T cell metabolic responses and disease tolerance to tuberculosis. *Sci Immunol.*
669 2018;3(23).
- 670 55. Rothchild AC, Jayaraman P, Nunes-Alves C, Behar SM. iNKT Cell Production of GM-CSF
671 Controls Mycobacterium tuberculosis. *PLoS Pathog.* 2014;10(1):e1003805.
- 672 56. Cambier CJ, O'Leary SM, O'Sullivan MP, Keane J, Ramakrishnan L. Phenolic Glycolipid
673 Facilitates Mycobacterial Escape from Microbicidal Tissue-Resident Macrophages. *Immunity.*
674 2017;47(3):552-65 e4.
- 675 57. Al Shammari B, Shiomi T, Tezera L, Bielecka MK, Workman V, Sathyamoorthy T, et al. The
676 Extracellular Matrix Regulates Granuloma Necrosis in Tuberculosis. *J Infect Dis.* 2015;212(3):463-
677 73.
- 678 58. Mishra BB, Lovewell RR, Olive AJ, Zhang G, Wang W, Eugenin E, et al. Nitric oxide
679 prevents a pathogen-permissive granulocytic inflammation during tuberculosis. *Nat Microbiol.*
680 2017;2:17072.
- 681 59. Sakai S, Kauffman KD, Sallin MA, Sharpe AH, Young HA, Ganusov VV, et al. CD4 T Cell-
682 Derived IFN-gamma Plays a Minimal Role in Control of Pulmonary Mycobacterium tuberculosis
683 Infection and Must Be Actively Repressed by PD-1 to Prevent Lethal Disease. *PLoS Pathog.*
684 2016;12(5):e1005667.

685 60. Roca FJ, Whitworth LJ, Redmond S, Jones AA, Ramakrishnan L. TNF Induces Pathogenic
686 Programmed Macrophage Necrosis in Tuberculosis through a Mitochondrial-Lysosomal-Endoplasmic
687 Reticulum Circuit. *Cell*. 2019;178(6):1344-61 e11.

688 61. Lerner TR, Borel S, Greenwood DJ, Repnik U, Russell MR, Herbst S, et al. Mycobacterium
689 tuberculosis replicates within necrotic human macrophages. *J Cell Biol*. 2017;216(3):583-94.

690 62. Cronan MR, Beerman RW, Rosenberg AF, Saelens JW, Johnson MG, Oehlers SH, et al.
691 Macrophage Epithelial Reprogramming Underlies Mycobacterial Granuloma Formation and Promotes
692 Infection. *Immunity*. 2016;45(4):861-76.

693 63. Elkington P, Lerm M, Kapoor N, Mahon R, Pienaar E, Huh D, et al. In Vitro Granuloma
694 Models of Tuberculosis: Potential and Challenges. *The Journal of infectious diseases*.
695 2019;219(12):1858-66.

696 64. Postow MA, Sidlow R, Hellmann MD. Immune-Related Adverse Events Associated with
697 Immune Checkpoint Blockade. *N Engl J Med*. 2018;378(2):158-68.

698 65. Elkington P, Tebruegge M, Mansour S. Tuberculosis: An Infection-Initiated Autoimmune
699 Disease? *Trends Immunol*. 2016;37(12):815-8.

700 66. Divangahi M, Khan N, Kaufmann E. Beyond Killing Mycobacterium tuberculosis: Disease
701 Tolerance. *Frontiers in immunology*. 2018;9:2976.

702 67. Olive AJ, Sasseti CM. Tolerating the Unwelcome Guest; How the Host Withstands Persistent
703 Mycobacterium tuberculosis. *Frontiers in immunology*. 2018;9:2094.

704 68. Elkington PT, Friedland JS. Permutations of time and place in tuberculosis. *Lancet Infect Dis*.
705 2015;15(11):1357-60.

706 69. Walker NF, Opondo C, Meintjes G, Jhilmeet N, Friedland JS, Elkington PT, et al. Invariant
707 Natural Killer T cell dynamics in HIV-associated tuberculosis. *Clin Infect Dis*. 2019.

708 70. Guzik K, Zak KM, Grudnik P, Magiera K, Musielak B, Törner R, et al. Small-Molecule
709 Inhibitors of the Programmed Cell Death-1/Programmed Death-Ligand 1 (PD-1/PD-L1) Interaction
710 via Transiently Induced Protein States and Dimerization of PD-L1. *Journal of Medicinal Chemistry*.
711 2017;60(13):5857-67.

712

713

714 **Figure Legends**

715 **Figure 1: PD-1 is expressed in human TB granulomas.** (A) Analysis of PD-1 expression by T cells
716 in the lung and peripheral circulation of thirty-five TB patients undergoing medically indicated lung
717 resection. PD-1 shows a trend towards higher expression by lung CD4⁺ (i) and is significantly higher
718 on lung CD8⁺ (ii) T cells. Significance analysed by one-tailed unpaired Mann-Whitney test. (B) Flow
719 cytometric analysis of lung parenchyma CD4⁺ (i) and CD8⁺ (ii) T cells from TB patients based on the
720 expression of PD-1, CD69 and CD103 demonstrates increased PD-1 expression in the resident T cells
721 in the lung parenchymal cells. Significance analysed by Kruskal-Wallis test with Dunn's multiple
722 comparison test. (C) Immunohistochemical staining for PD-1⁺, CD4⁺ and CD8⁺ expression in human
723 lung TB granulomas. PD-1 is expressed around the central macrophage core in the same region as
724 CD4⁺ (ii) and CD8⁺ (iii) T cells. Co-localization of PD-1 (blue), CD4⁺ (red) and CD8⁺ (yellow) using
725 false colour of the immunostaining shows co-localisation of PD-1 with both CD4⁺ and CD8⁺ cells
726 (purple and green respectively) (iv). Scale bar 100µm. (D) PD-1 is not expressed in caseating
727 granulomas where immunopathology is present in human lung biopsies (i). Six biopsies taken as part
728 of routine clinical care were studied. CD4⁺ (ii) and CD8⁺ (iii) expressing cells are present in the same
729 area, and so absence of PD-1 immunoreactivity is not due to lack of viable cells. Scale bar 200µm.

730 **Figure 2: The PD-1/ PD-L1 axis is upregulated in the 3D TB granuloma system.** (A) Still images
731 from time-lapse microscopy imaging demonstrating increasing cellular aggregation of PBMC around
732 a focus of ultraviolet killed Mtb H37Rv in the 3D granuloma system at times 0, 12, 24 and 48h post
733 encapsulation in the matrix. The Z projection shows the cells contained within the designated volume
734 in a 2D reconstruction. Full time course in Video 1. (B) Gene expression of PD-1 and its ligands in
735 the 3D microsphere model. RNA was extracted from live Mtb-infected PBMC and relative expression
736 investigated by qRT-PCR at day 4 post infection. Open bars, normoxia, filled bars 1% hypoxia. PD-
737 L1 and PD-L2 are upregulated by Mtb infection, and in 1% hypoxia PD-1 expression is increased and
738 PD-L2 expression further augmented (n=4). Results are normalised against the housekeeping genes
739 GAPDH, β-Microbulin and FANTA and showed similar results. β-microglobulin used for (B).
740 *p<0.05, **p<0.01. (C-E) Surface expression of PD-1 and PD-L1. PBMCs were decapsulated from

741 Mtb-infected microspheres at day 7 and surface expression of PD-1 and its ligand PD-L1 were
742 analysed by flow cytometry. PD-1 is expressed in CD4⁺ (C) and CD8⁺ (D) T cells in PBMC from Mtb
743 infected microspheres incubated in normoxia. PD-1 expression was significantly upregulated in 1%
744 hypoxia. Representative flow cytometry plots and level of expression of PD-1 by the CD4⁺ and CD8⁺
745 T cell fractions are shown (n=4). (E) PD-L1 expression on CD14⁺CD11b⁺ cells within PBMC in Mtb
746 infected microspheres is upregulated in both normoxia and 1% hypoxia at day 7 (n=4). Significance
747 of *p<0.05. (F) Growth of Mtb H37Rv ffLux⁺ in microspheres in normoxia and 1% hypoxia
748 measured at day 3, 7 and 14. Hypoxia reduces Mtb growth. (G) Hypoxia inducible factor 1 α (HIF-
749 1 α) mRNA levels were increased in Mtb-infected microspheres incubated in 1% hypoxia. RNA was
750 extracted from decapsulated microspheres and normalised to uninfected microspheres in the same
751 environment. Results were normalised to the housekeeping genes GAPDH, β -microglobulin and
752 FANTA to check the housekeeping gene are not affected by hypoxia. Similar results all three of the
753 housekeeping genes. β -microglobulin used for this graph. Significance *** p<0.001.

754 **Figure 3: PD-1 pathway inhibition increases Mtb growth.** (A) Inhibition of PD-1 receptors by
755 small chemical inhibitor 1 increases Mtb growth in a dose-response manner (1-1000nM). Inhibitor
756 concentration 1nM (green), 10nM (purple), 100nM (blue) and 1 μ M (red). (B) Inhibitor 1 was not
757 toxic to Mtb-infected PBMC, analysed by CytoTox-Glo assay (Day 7). (C) Cellular toxicity was no
758 different at day 14 as analysed by LDH release. Concentration 1 and 1000nM were analysed for
759 toxicity. (D) Spartalizumab, a therapeutic monoclonal anti-PD-1 antibody, progressively increased
760 Mtb growth in microspheres in normoxia in a dose-dependent manner. (E) Spartalizumab also
761 increased Mtb growth in hypoxia. Media (black), isotype (blue), spartalizumab 20 μ g/ml (green) and
762 200 μ g/ml (red). (F) The anti-PD-1 antibody had no effect on cell survival in microspheres in
763 normoxia (clear bars) and 1% hypoxia (filled bars). Cytotoxicity is determined by measuring LDH
764 release at day 14 and normalized by the control. ****p<0.0001.

765 **Figure 4: PD-1 inhibition increases secretion of multiple cytokines and growth factors.** PD-1/PD-
766 L1 signalling was inhibited by Spartalizumab, a humanized IgG4 anti-PD1 monoclonal antibody, in
767 Mtb-infected microspheres at 20 and 200 μ /ml in normoxia. Supernatants were collected at day 14 and

768 accumulation of cytokines and growth factors was analysed by Luminex 35-multiplex assay.
769 Concentrations were normalized to secretion by Mtb infected microspheres to demonstrate relative
770 fold change, and individual concentrations are shown in Supplementary figure 6. The experiment was
771 performed twice with three replicates. Red font: ** $p < 0.001$ for Spartalizumab versus isotype
772 control.

773 **Figure 5: Addition of TNF- α increases Mtb growth in microspheres in normoxia.** Recombinant
774 human G-CSF, GM-CSF, IL-4, IL-6, IL-10, IL-12, TNF- α , IL-1RA, MIP-1 α , MIP-1 β or RANTES
775 were added either individually (**A** and **B**) or in combination pools (**C**) to Mtb-infected microspheres at
776 “low” concentrations, defined as that measured in media around spheres after anti-PD-1 treatment.
777 Recombinant human TNF- α increases growth of Mtb, whilst other pro-inflammatory cytokines did
778 not (**A**). GM-CSF has a lesser growth-promoting effect (**B**). The only combination pool that
779 increased Mtb growth was the pro-inflammatory cytokine pool, containing TNF- α (**C**). (**D**) TNF- α
780 results in a dose-dependent increase in the Mtb growth over time. (**E**) Anti-TNF- α neutralising
781 antibodies partially suppress the increased Mtb growth caused by TNF- α augmentation. Anti-TNF- α
782 from Thermo Fisher Scientific. (**F**) Anti-PD1 antibody incorporation within microspheres increases of
783 Mtb growth at day 7, and this effect is reversed by concurrent anti-TNF- α neutralising antibodies
784 within microspheres. The constituent of the cytokine pools are: Growth factor pool (GF: GM-CSF and
785 G-CSF), Anti-Inflammatory cytokine pool (Anti-Inf: IL-10 and IL-1RA), Pro-Inflammatory cytokine
786 pool (Pro-Inf: TNF- α , IL-6 and IL-12) and Chemokine pool (Chemo: RANTES, MIP-1 α , MIP-1 β).

787 **Figure 6: TNF- α is expressed in human TB granulomas and sputum TNF- α concentrations**
788 **negatively correlate with circulating PD-1 expression.** (**A**) TNF- α is expressed within human lung
789 TB granulomas, with greater immunoreactivity than control lung tissue at the excision margin of lung
790 cancer (i & ii). Quantification of TNF- α immunostaining (n=5) in TB cases was significantly higher
791 than controls (n=5) (iii). (**B**) TNF- α immunostaining was extensive in the lung granuloma of a
792 patient that developed TB whilst treated with pembrolizumab, a humanized anti-PD-1 antibody (n=1).
793 (**C**) CD4⁺ T cell PD-1 expression on circulating PBMC negatively correlates with sputum TNF- α
794 concentration in a separate cohort where paired sputum and PBMCs samples are available. Green

795 dots, healthy controls; Black TB cases; Orange respiratory symptomatics. Analysis by Spearman's
796 correlation analysis gave r-value of -0.341 with p=0.0484

797

798 **Figure supplement legends**

799

800 **Figure 1–figure supplement 1:** PD-1 expression on peripheral CD4⁺ and CD8⁺ T-cells is
801 predominantly on CD103- and CD69-negative cells. Significance was analyzed by one-tailed
802 unpaired Mann-Whitney test.

803 **Figure 1–figure supplement 2:** PD-1 expressing cells are absent in the immediate region surrounding
804 caseous necrosis in human TB granulomas. Images from four different clinical samples are presented.
805 Scale bar 100µm.

806 **Figure 2–figure supplement 1:** Hypoxia alone has no significant effect on expression of the PD-
807 1/PDL-1/2 axis. Gene expression PD-1 and its ligands in uninfected cells was compared between
808 normoxic and hypoxic conditions in the microsphere model. RNA was extracted from uninfected
809 PBMCs and relative expression investigated by qRT-PCR at day 4. Open bars PD-1, filled bars PD-
810 L1 and black bars PD-L2 respectively. Results were normalised against the housekeeping genes
811 GAPDH, β-Microbulin and FANTA and showed similar results. No significant changes in gene
812 expression were noted in uninfected microspheres. β-microglobulin used for the analysis presented.

813 **Figure 2–figure supplement 2:** (A) Mtb H37Rv ffluc⁺ growth in 1% hypoxia. Microspheres were
814 decapsulated in a media containing 5mM EDTA and 0.1% saponin at day 14. The lysate was
815 centrifuged, re-suspended in 1ml PBS, serially diluted and grown in Middlebrook 7H11 media for 3
816 weeks before colony counting. (B) Host cell viability using 3D CytoxGlo viability assay (Promega)
817 shows no significant difference between normoxia (open bars) and hypoxia (filled bars) at day 4 and
818 day 7.

819 **Figure 3–figure supplement 1:** Small chemical inhibition of PD-1/PD-L1 interaction in 1% hypoxia
820 measured at day 14 shows a dose-dependent increase in Mtb growth with PD-1 inhibition. ***
821 $p < 0.0001$ with one-way ANOVA with Dunnett’s multiple comparison test.

822 **Figure 4–figure supplement 1:** Cytokine accumulation around microspheres after inhibition of PD-
823 1/PD-L1 signalling with Spartalizumab, a humanized IgG4 anti-PD1 monoclonal antibody at 20 and
824 200 μ g/ml in normoxia (N) and 1% hypoxia (H). Supernatants were collected at day 14 and a Luminex
825 35-multiplex assay was performed. The experiment was performed twice with three replicates.
826 Concentrations are in pg/ml. Labels in red correspond to significantly raised cytokine values. Red
827 font: Significance ** $p < 0.001$.

828 **Figure 4–figure supplement 2:** PD-1 inhibition increases secretion of multiple cytokines and growth
829 factors in 1% hypoxia. Supernatants were collected at day 14 and accumulation of cytokines and
830 growth factors was analysed by Luminex 35-multiplex assay. Concentrations were normalized to
831 secretion by Mtb infected microspheres to demonstrate relative fold change, and individual
832 concentrations are shown in Supplementary figure 5. The experiment was performed twice with three
833 replicates. Red font: ** $p < 0.001$ for Spartalizumab versus Isotype control.

834 **Figure 4–figure supplement 3:** Spartalizumab induces TNF- α secretion in uninfected and infected
835 microspheres, which is neutralised by anti-TNF- α . PBMCs which were uninfected or infected with
836 Mtb were encapsulated in alginate-collagen matrix after pre- incubation in Spartalizumab at
837 200 μ g/ml. The supernatant was collected to measure TNF- α secretion at day 7. (A) Spartalizumab
838 induces TNF- α secretion in uninfected cells above background, which is accentuated with Mtb
839 infection. (B) Anti-PD-1 antibody increases TNF- α secretion from Mtb infected cells above isotype,
840 and the detectable levels are suppressed by anti-TNF antibody (50 μ g/ml).

841 **Figure 5–figure supplement 1:** Individual Mtb growth curves at “high” cytokine concentration, five
842 times the concentration measured in media after anti-PD-1 treatment. Human recombinant G-CSF,
843 GM-CSF, IL-4, IL-6, IL-10, IL-12, TNF- α , IL-1RA, MIP-1 α , MIP-1 β and RANTES were added to
844 microspheres either individually or in combination pools to microspheres at 5 times the concentrations

845 in Figure 5, determined by the concentration measured in the media around the microspheres. TNF- α
846 increases Mtb growth in microspheres alone and in the pro-inflammatory pool.

847 **Figure 5–figure supplement 2:** Anti-TNF- α neutralizing antibodies suppress the Mtb growth
848 following TNF- α from a different source (Anti-TNF- α from Sigma-Aldrich, UK).

849 **Figure 5–figure supplement 3:** TNF- α skews polarization of monocytes to macrophages with lower
850 CD80 expression. PBMCs were infected with Mtb H37Rv at MOI of 0.1 and encapsulated in alginate-
851 collagen microspheres after overnight incubation. Microspheres were then incubated in complete
852 RPMI (with L-Glutamine and 10% human serum) with TNF- α 7.5ng/ml. Uninfected PBMCs were
853 encapsulated and treated similarly as a comparator for TNF- α stimulation. At day 7, the microspheres
854 were decapsulated in 0.5mM EDTA solution at pH of 7.2. Double staining with CD14 and CD11b
855 defined macrophages, which were classified by CD80 and CD163 expression. (A) Histogram showing
856 expression of CD163 and CD80 where there was significant decrease in CD80 expression as shown in
857 Figure (B). TNF suppressed the relative geometric mean of CD80, but did not affect CD163
858 expression. This experiment was performed in 4 separate donors.

859 **Figure 5–figure supplement 4:** Hierarchical gating strategy used to identify lymphocyte and
860 monocytic populations from decapsulated microspheres containing human peripheral blood
861 monocular cells. Single cells were decapsulated from microspheres in 5mM EDTA, washed and
862 processed for flow cytometry. First doublets were excluded from live cells, then cells were gated as
863 CD3+ and CD3- . Subsequently, lymphocytes were further classified into CD4+ and CD8+, which are
864 sub-categorized based on PD-1 staining. Double staining with both CD14 and CD11b defined
865 macrophages, which were further analysed for PD-L1, CD80 and CD163 surface expression. All the
866 antibodies and clone number are listed in the text and the key resources table.

867

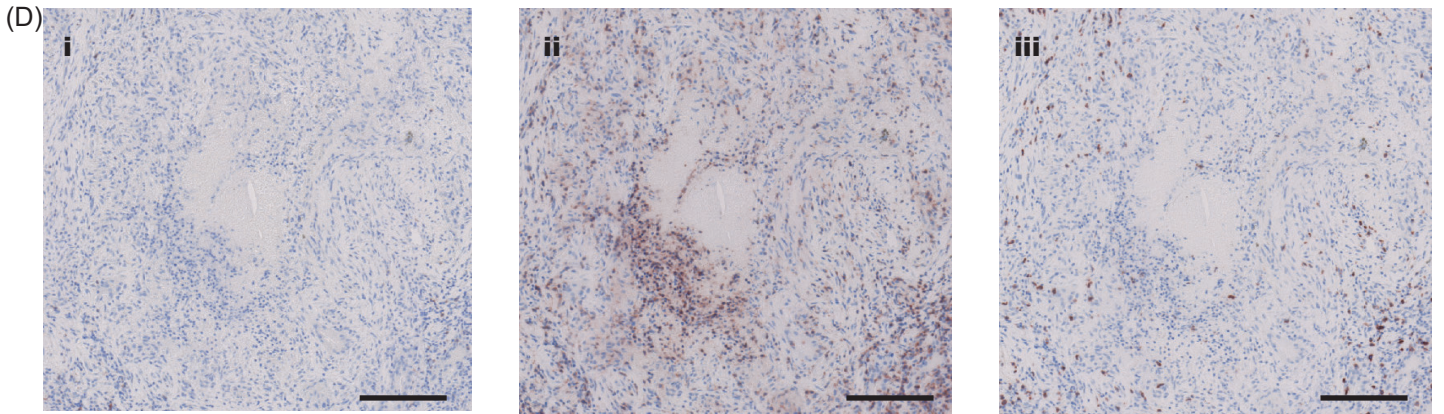
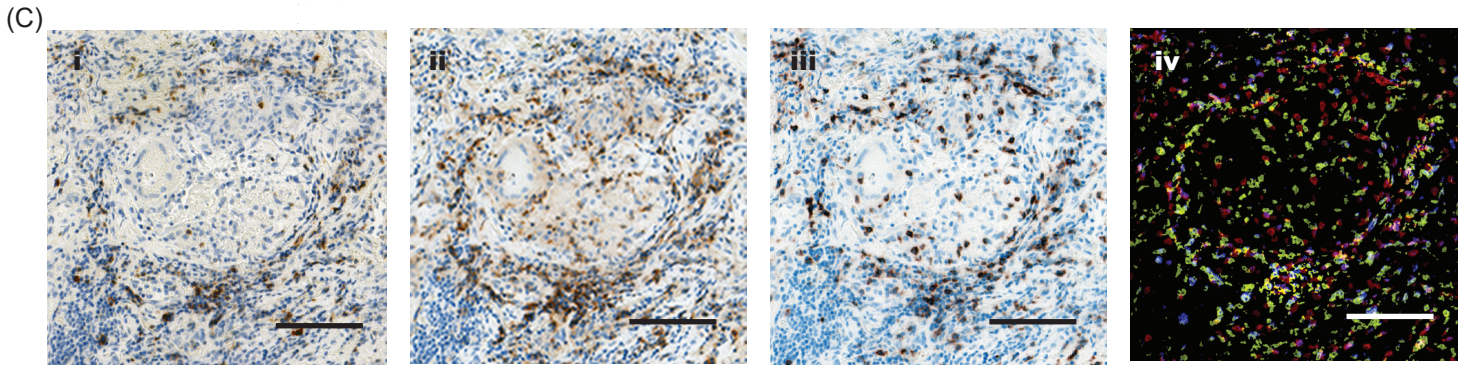
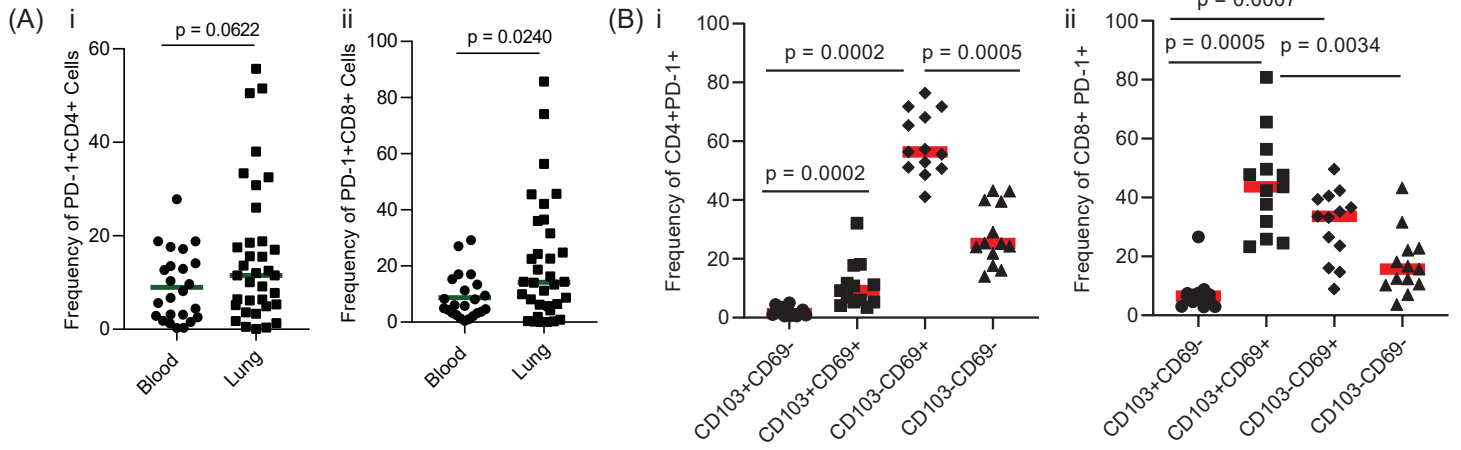
868 **Supplementary file 1:** PD-1 expressing cells for each subset expressed as percentage of live CD45+
869 cells, with range in parentheses.

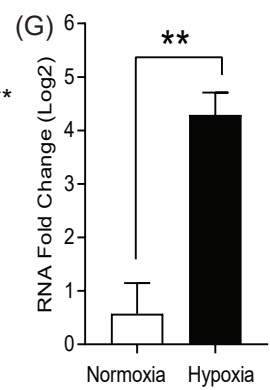
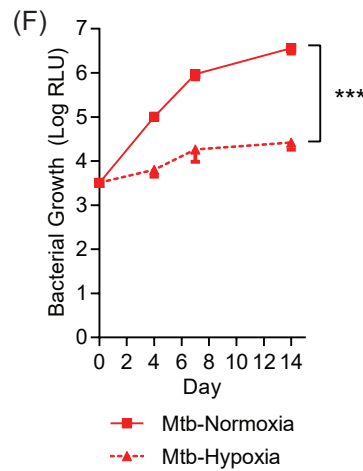
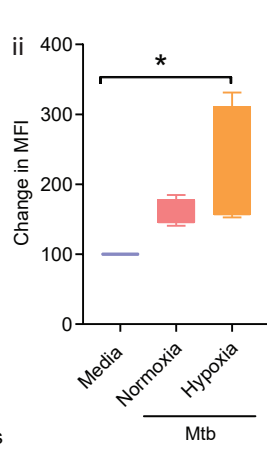
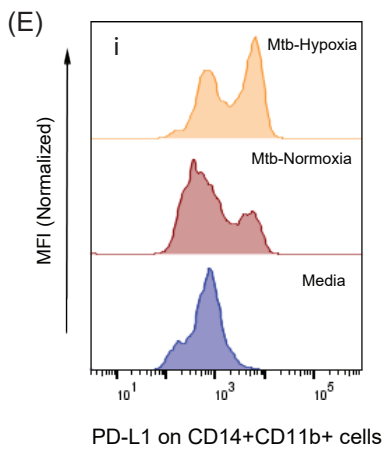
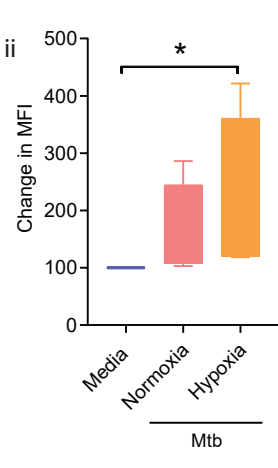
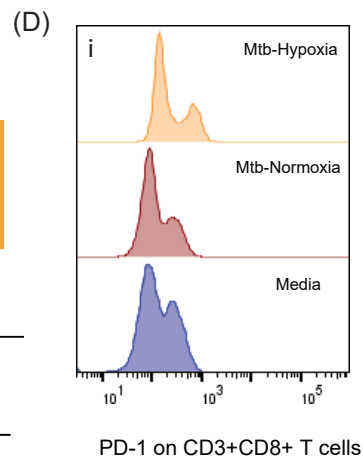
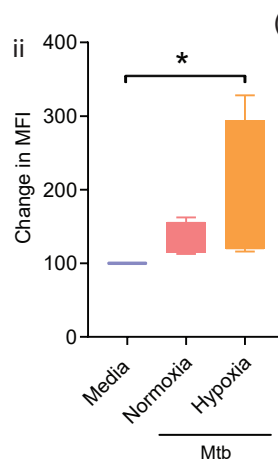
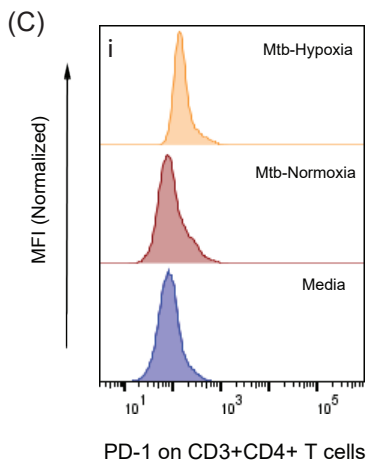
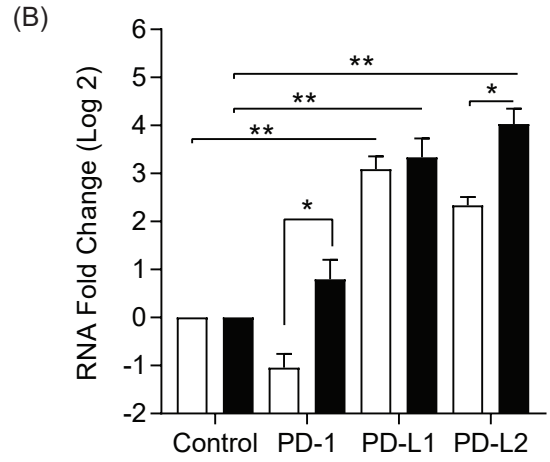
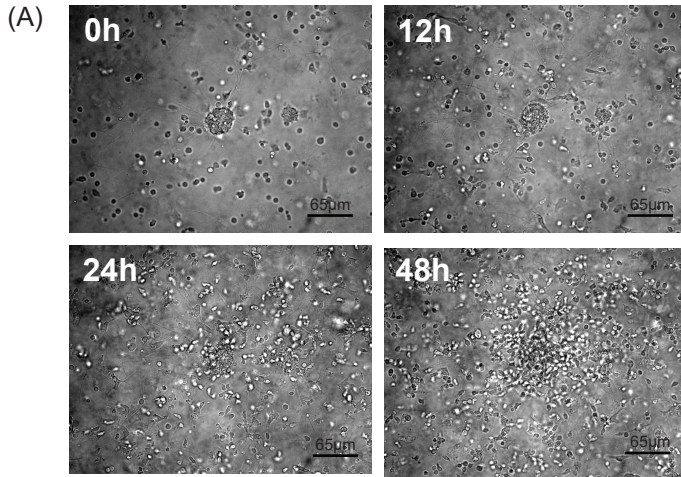
870

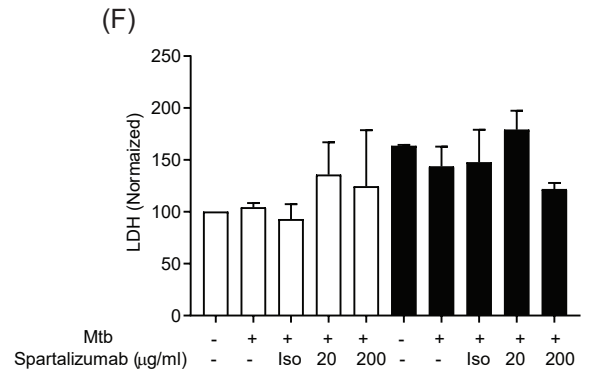
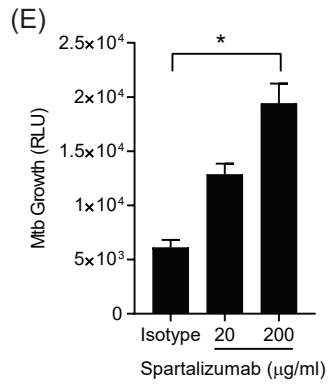
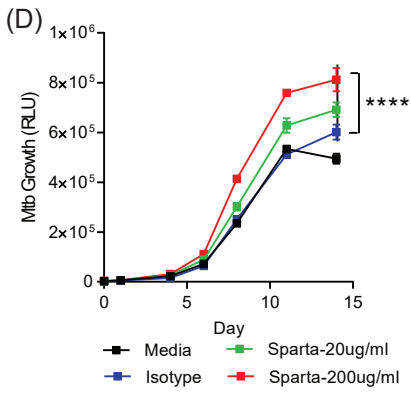
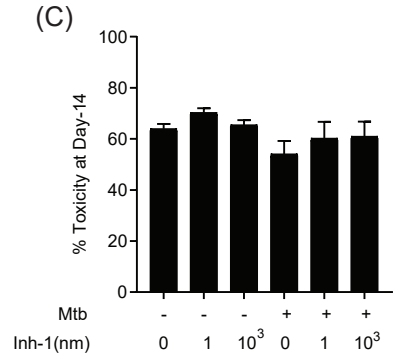
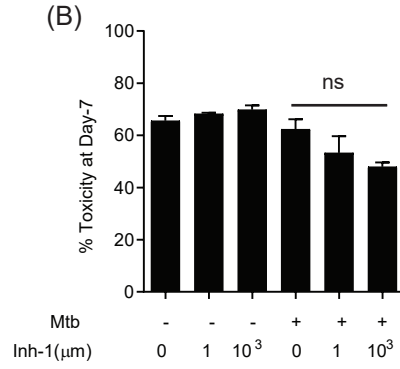
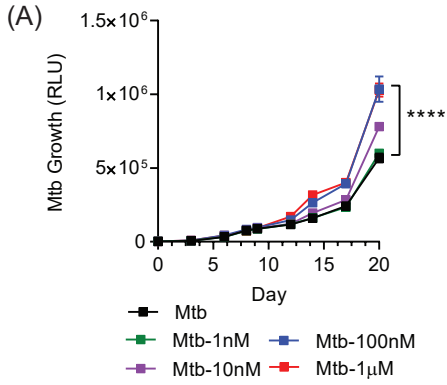
871 **Video 1:** Cell migration over 48 hours around a central cluster of
872 macrophages infected with UV-killed Mtb within a 3D alginate-collagen matrix. Migration is seen in
873 the first 24 hours, without aggregation, and then progressive granuloma formation occurs.

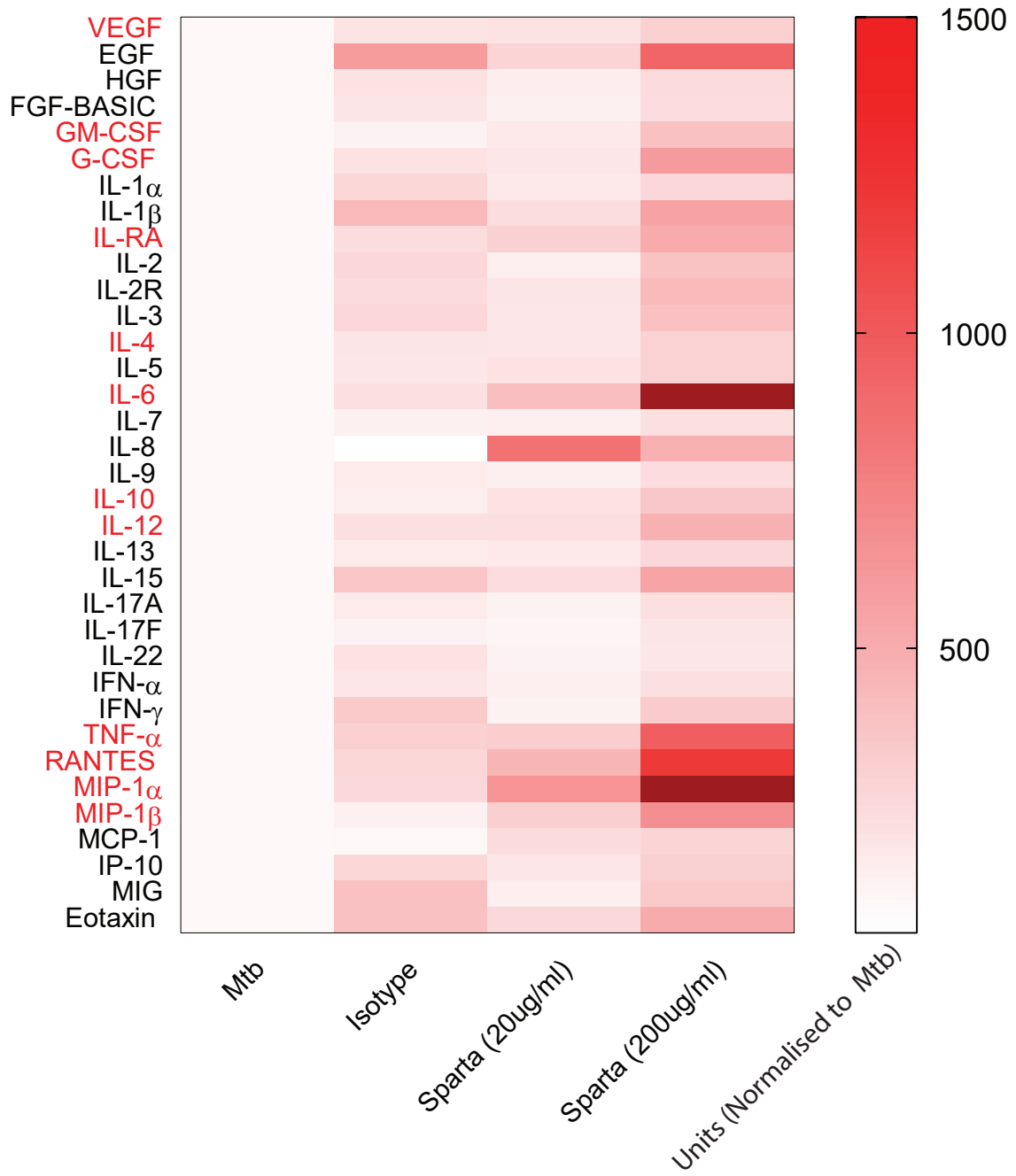
874

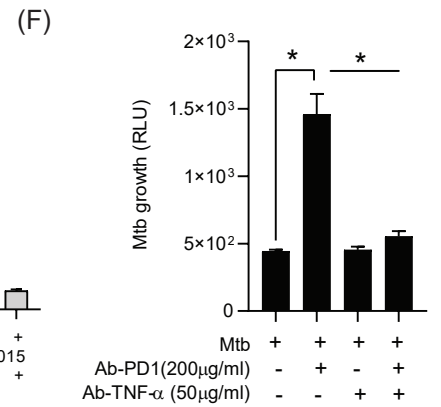
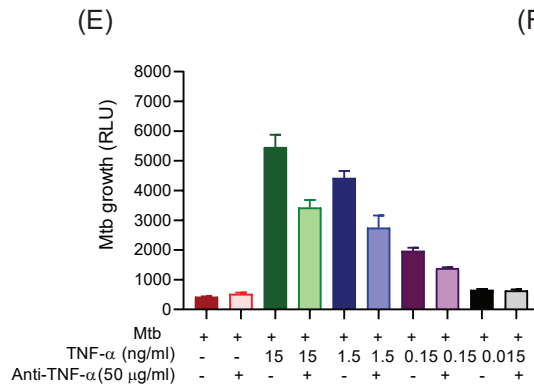
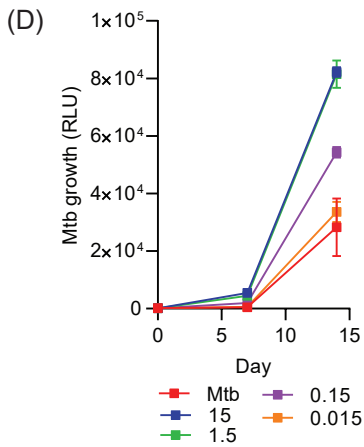
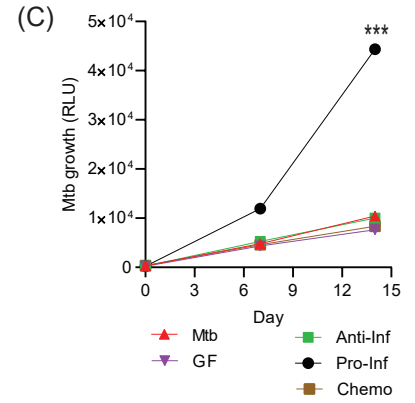
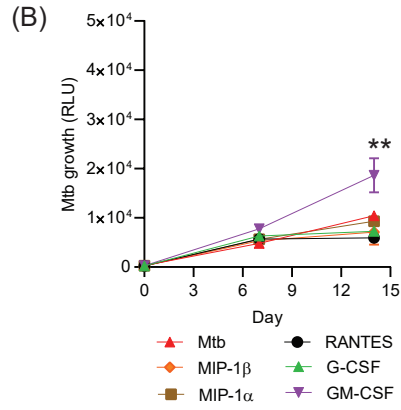
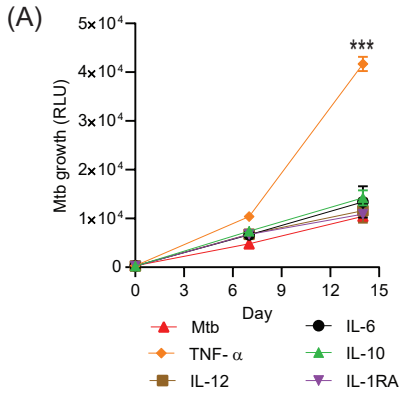
875

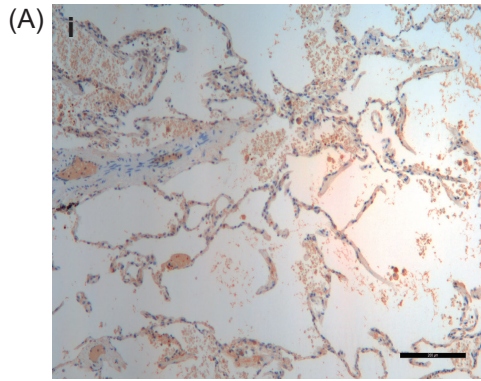




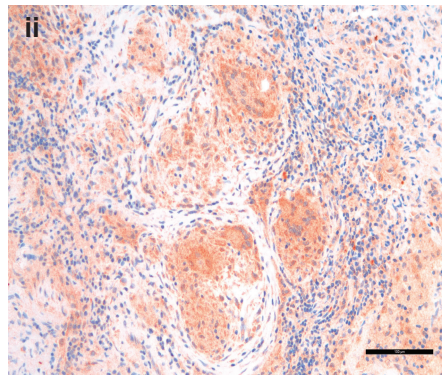




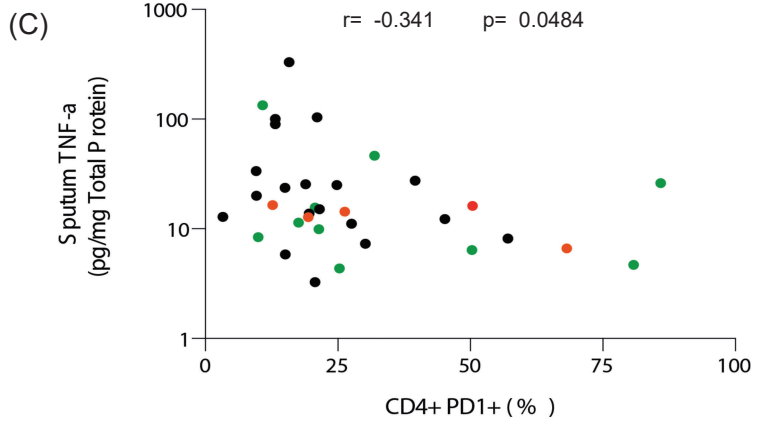
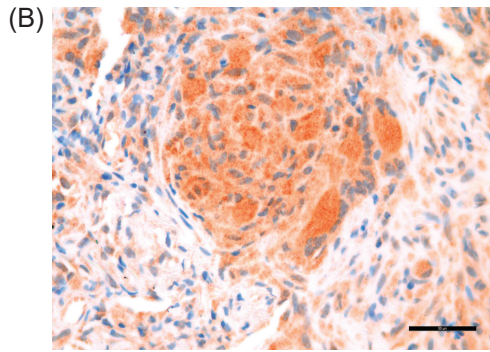
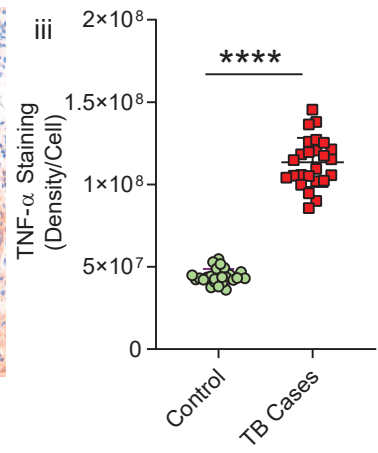




Lung cancer



TB



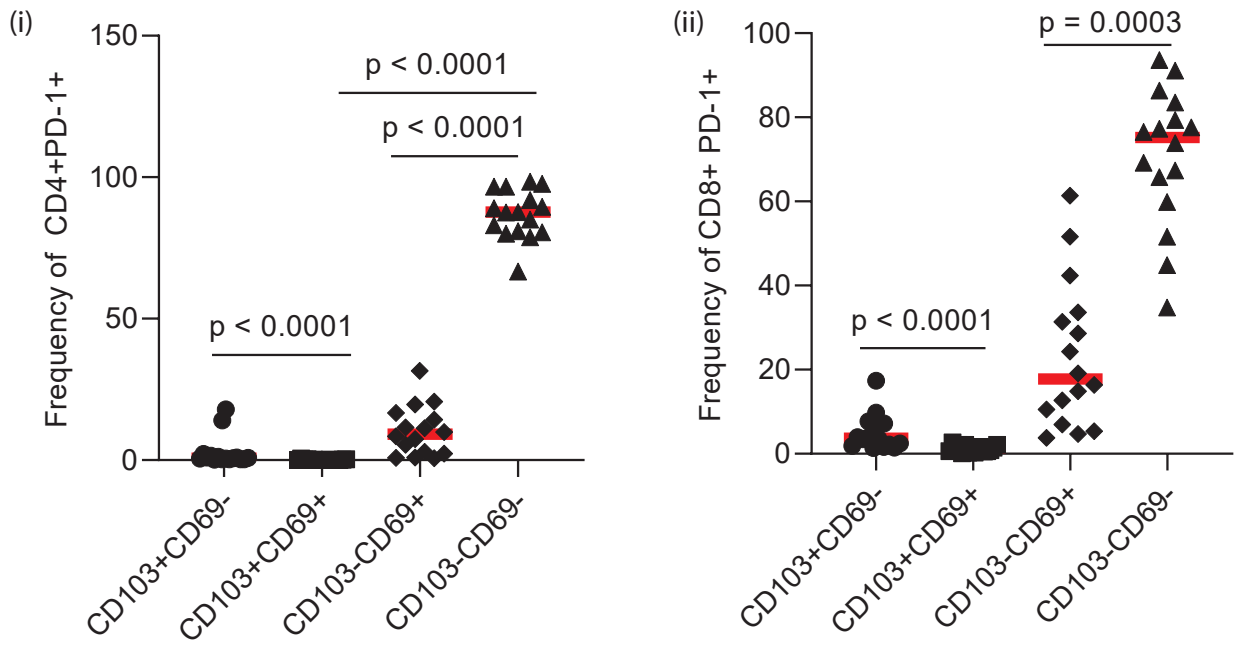


Figure 1–figure supplement 1: PD-1 expression on peripheral CD4⁺ and CD8⁺ T-cells is predominantly on CD103- and CD69-negative cells. Significance was analyzed by one-tailed unpaired Mann-Whitney test.

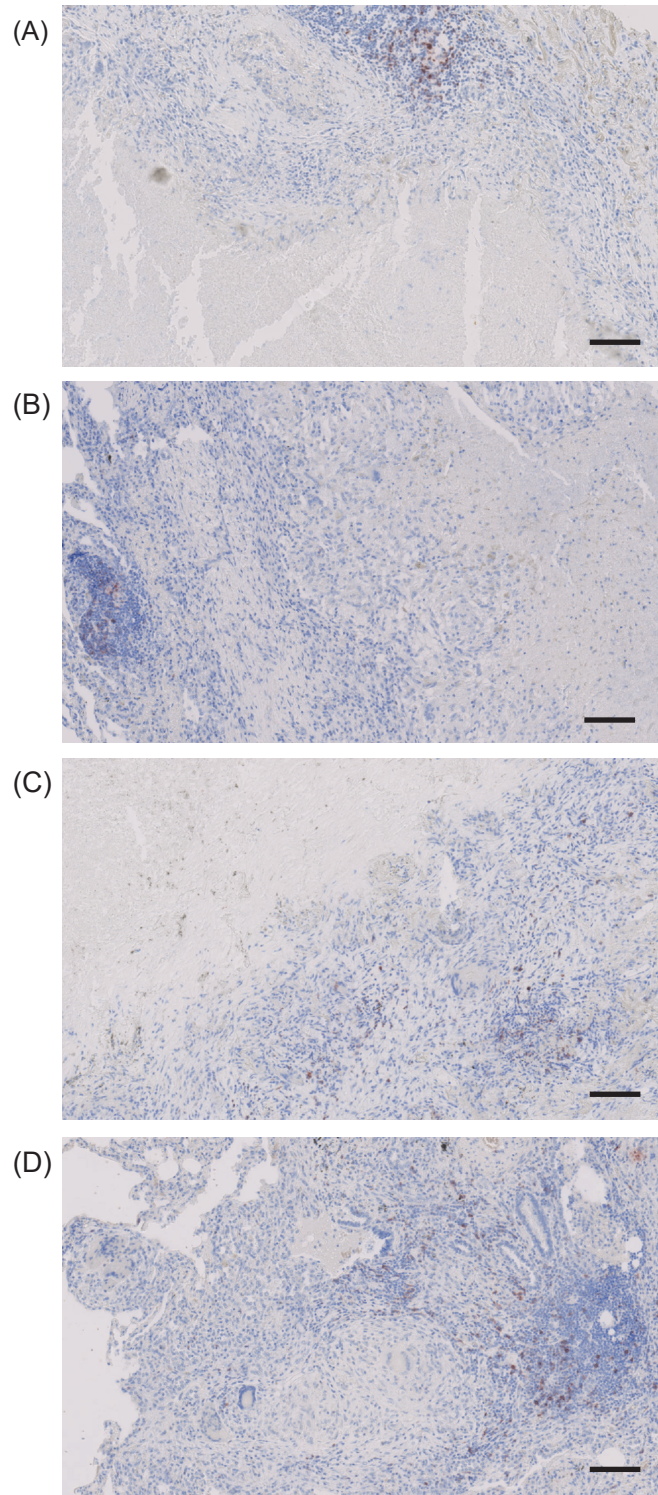


Figure 1–figure supplement 2: PD-1 expressing cells are absent in the immediate region surrounding caseous necrosis in human TB granulomas. Images from four different clinical samples are presented. Scale bar 100 μ m.

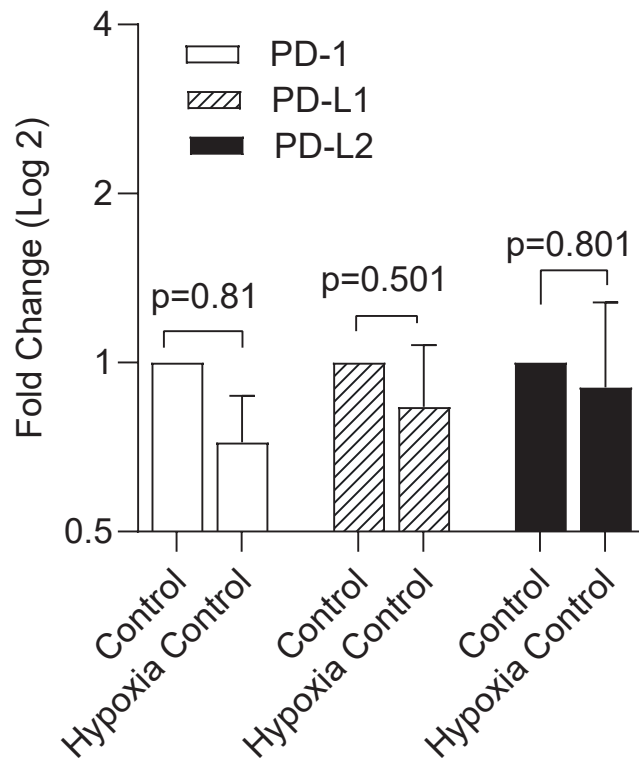


Figure 2–figure supplement 1: Hypoxia alone has no significant effect on expression of the PD-1/PDL-1/2 axis. Gene expression PD-1 and its ligands in uninfected cells was compared between normoxic and hypoxic conditions in the microsphere model. RNA was extracted from uninfected PBMCs and relative expression investigated by qRT-PCR at day 4. Open bars PD-1, filled bars PD-L1 and black bars PD-L2 respectively. Results were normalised against the housekeeping genes GAPDH, β -Microbulin and FANTA and showed similar results. No significant changes in gene expression were noted in uninfected microspheres. β -microglobulin used for the analysis presented.

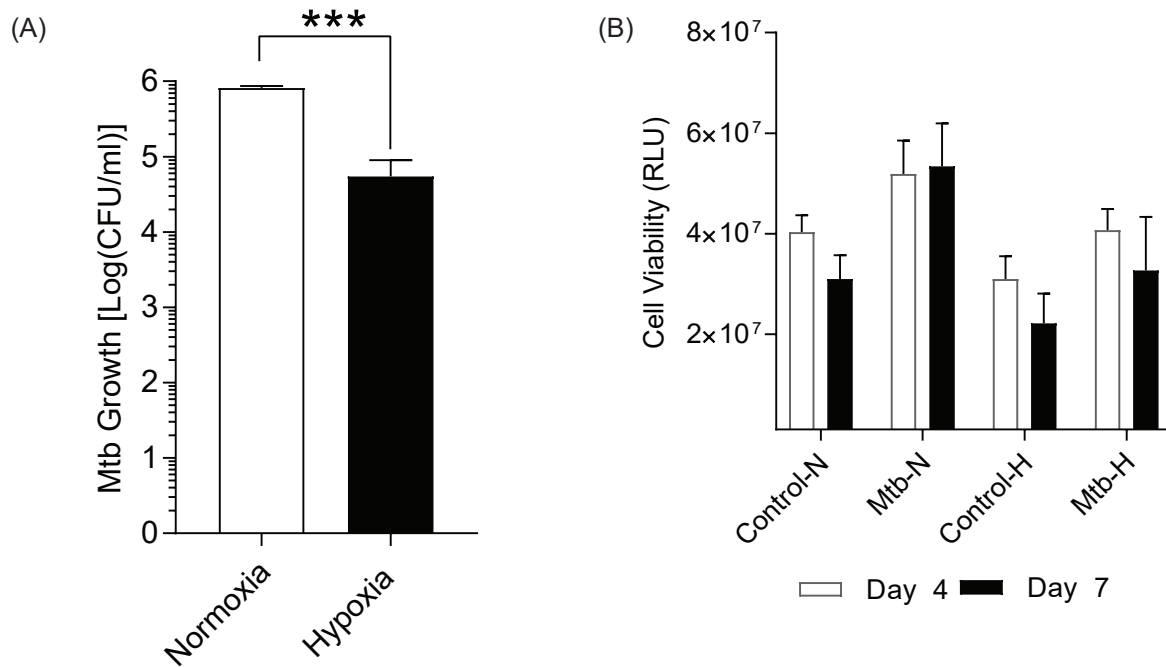


Figure 2–figure supplement 2A: (A) Mtb H37Rv ffluc+ growth in 1% hypoxia. Microspheres were decapsulated in a media containing 5mM EDTA and 0.1% saponin at day 14. The lysate was centrifuged, re-suspended in 1ml PBS, serially diluted and grown in Middlebrook 7H11 media for 3 weeks before colony counting. (B) Host cell viability using 3D CyttoxGlo viability assay (Promega) shows no significant difference between normoxia (open bars) and hypoxia (filled bars) at day 4 and day 7.

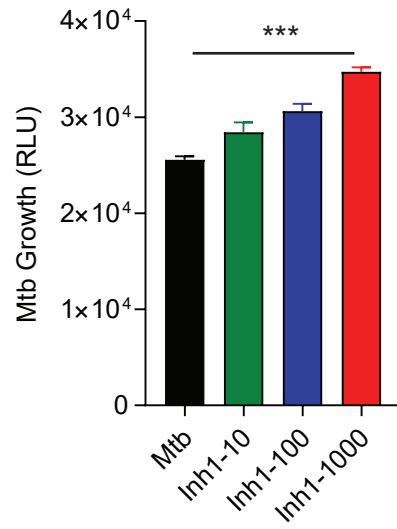


Figure 3–figure supplement 1: Small chemical inhibition of PD-1/PD-L1 interaction in 1% hypoxia measured at day 14 shows a dose-dependent increase in Mtb growth with PD-1 inhibition. *** $p < 0.0001$ with one-way ANOVA with Dunnett's multiple comparison test.

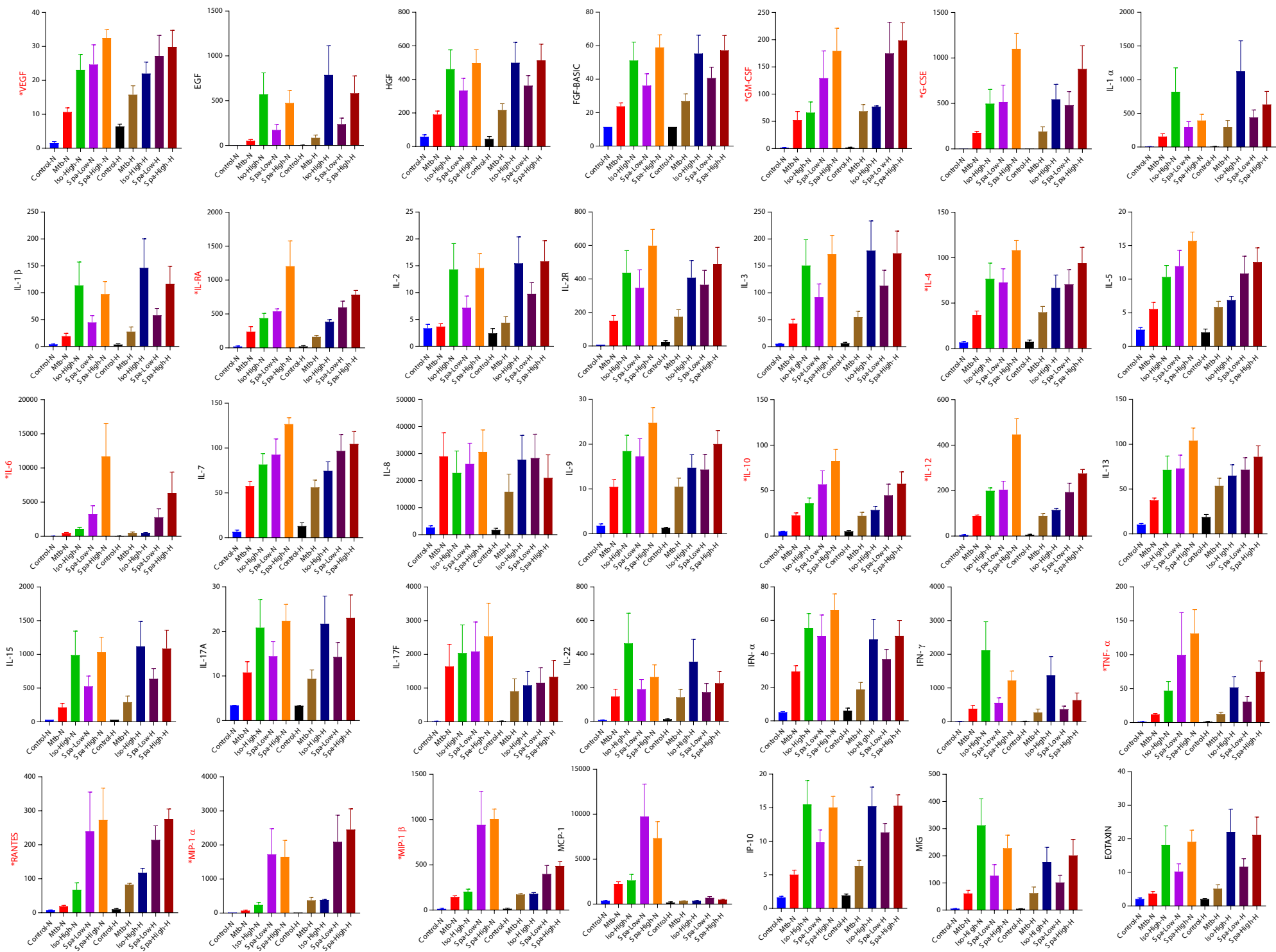


Figure 4-figure supplement 1 (legend overleaf)

Figure 4–figure supplement 1: Cytokine accumulation around microspheres after inhibition of PD-1/PD-L1 signalling with Spartalizumab, a humanized IgG4 anti-PD1 monoclonal antibody at 20 and 200µg/ml in normoxia (N) and 1% hypoxia (H). Supernatants were collected at day 14 and a Luminex 35-multiplex assay was performed. The experiment was performed twice with three replicates. Concentrations are in pg/ml. Labels in red correspond to significantly raised cytokine values. Red font: Significance **p<0.001.

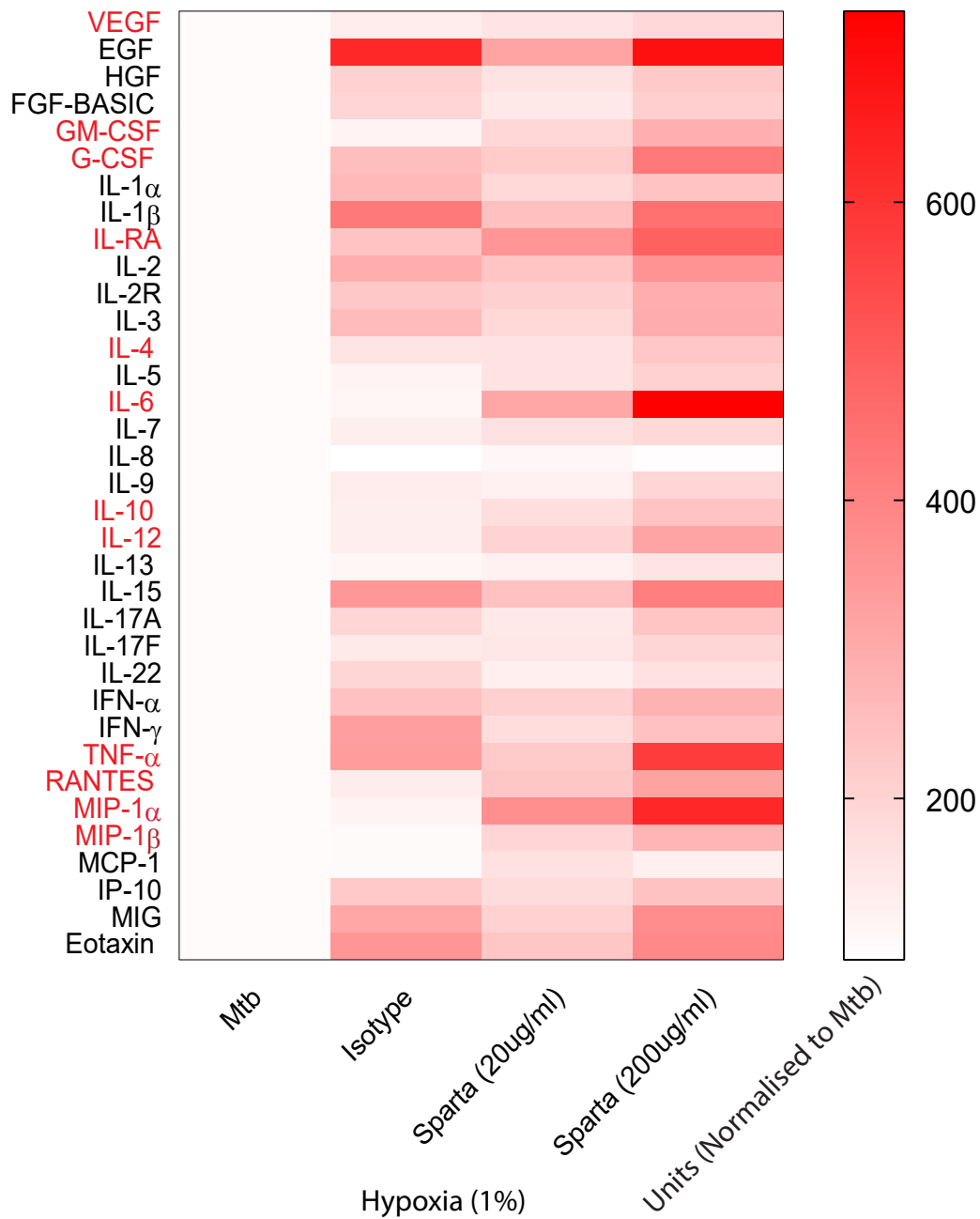


Figure 4–figure supplement 2: PD-1 inhibition increases secretion of multiple cytokines and growth factors in 1% hypoxia. Supernatants were collected at day 14 and accumulation of cytokines and growth factors was analysed by Luminex 35-multiplex assay. Concentrations were normalized to secretion by Mtb infected microspheres to demonstrate relative fold change, and individual concentrations are shown in Supplementary figure 5. The experiment was performed twice with three replicates. Red font: ** p < 0.001 for Spartalizumab versus Isotype control.

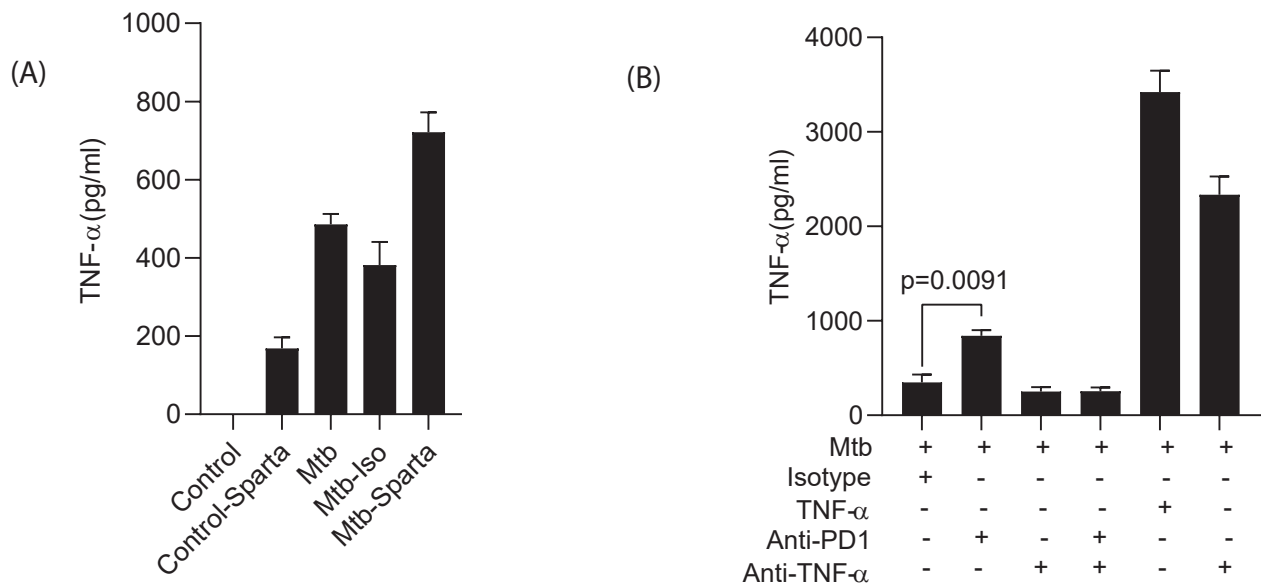


Figure 4—figure supplement 3: Spartzalizumab induces TNF- α secretion in uninfected and infected microspheres, which is neutralised by anti-TNF- α . PBMCs which were uninfected or infected with Mtb were encapsulated in alginate-collagen matrix after pre- incubation in Spartzalizumab at 200 μ g/ml. The supernatant was collected to measure TNF- α secretion at day 7. (A) Spartzalizumab induces TNF- α secretion in uninfected cells above background, which is accentuated with Mtb infection. (B) Anti-PD-1 antibody increases TNF- α secretion from Mtb infected cells above isotype, and the detectable levels are suppressed by anti-TNF antibody (50 μ g/ml).

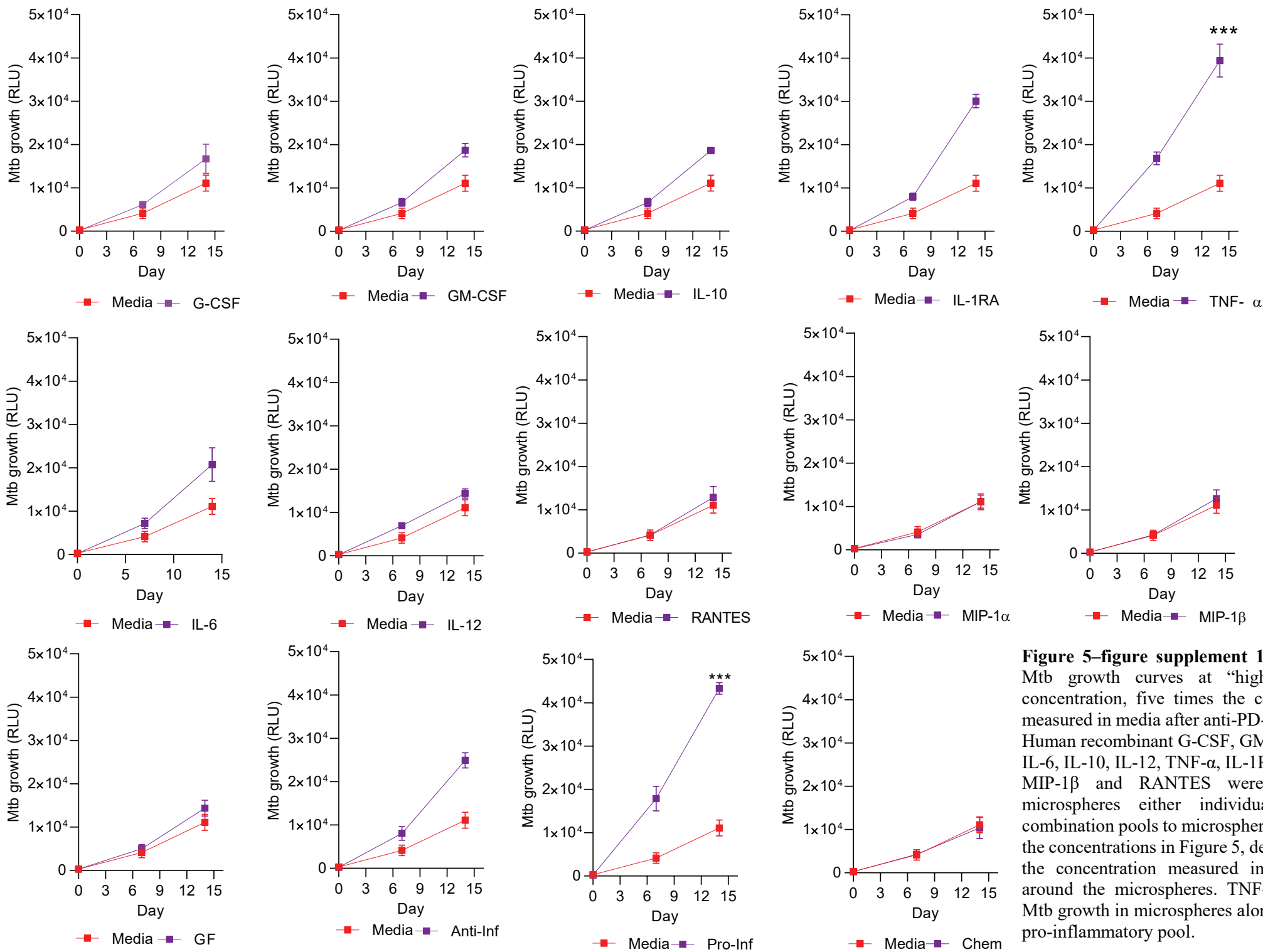


Figure 5-figure supplement 1: Individual Mtb growth curves at “high” cytokine concentration, five times the concentration measured in media after anti-PD-1 treatment. Human recombinant G-CSF, GM-CSF, IL-4, IL-6, IL-10, IL-12, TNF- α , IL-1RA, MIP-1 α , MIP-1 β and RANTES were added to microspheres either individually or in combination pools to microspheres at 5 times the concentrations in Figure 5, determined by the concentration measured in the media around the microspheres. TNF- α increases Mtb growth in microspheres alone and in the pro-inflammatory pool.

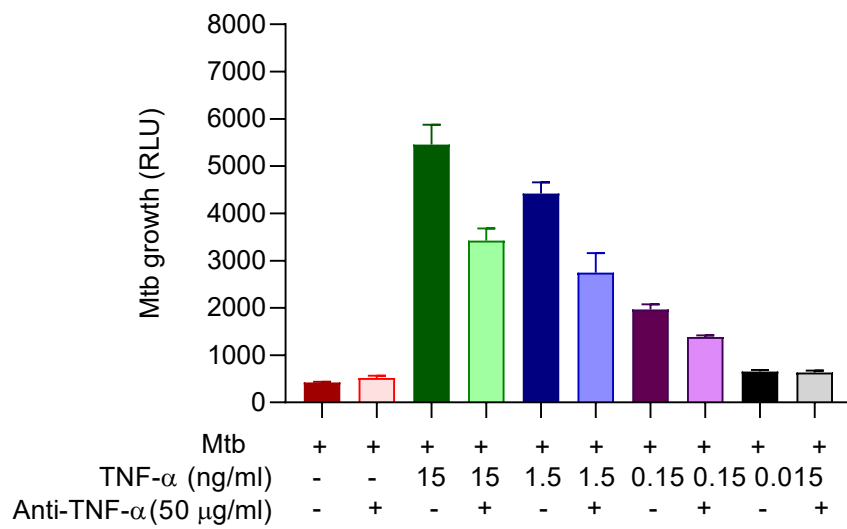


Figure 5–figure supplement 2: Anti-TNF- α neutralizing antibodies suppress the Mtb growth following TNF- α from a different source (Anti-TNF- α from Sigma-Aldrich, UK).

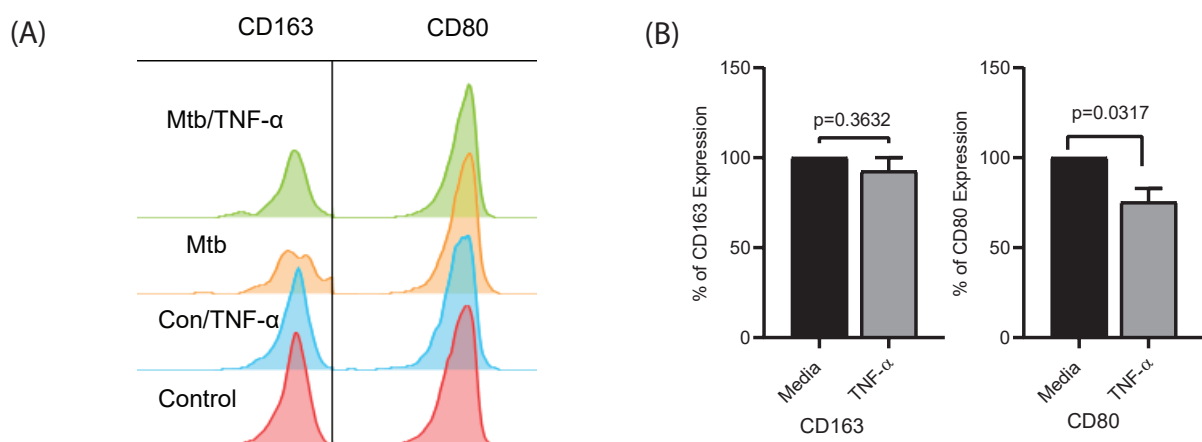


Figure 5–figure supplement 3: TNF- α skews polarization of monocytes to macrophages with lower CD80 expression. PBMCs were infected with Mtb H37Rv at MOI of 0.1 and encapsulated in alginate-collagen microspheres after overnight incubation. Microspheres were then incubated in complete RPMI (with L-Glutamine and 10% human serum) with TNF- α 7.5ng/ml. Uninfected PBMCs were encapsulated and treated similarly as a comparator for TNF- α stimulation. At day 7, the microspheres were decapsulated in 0.5mM EDTA solution at pH of 7.2. Double staining with CD14 and CD11b defined macrophages, which were classified by CD80 and CD163 expression. (A) Histogram showing expression of CD163 and CD80 where there was significant decrease in CD80 expression as shown in Figure (B). TNF suppressed the relative geometric mean of CD80, but did not affect CD163 expression. This experiment was performed in 4 separate donors.

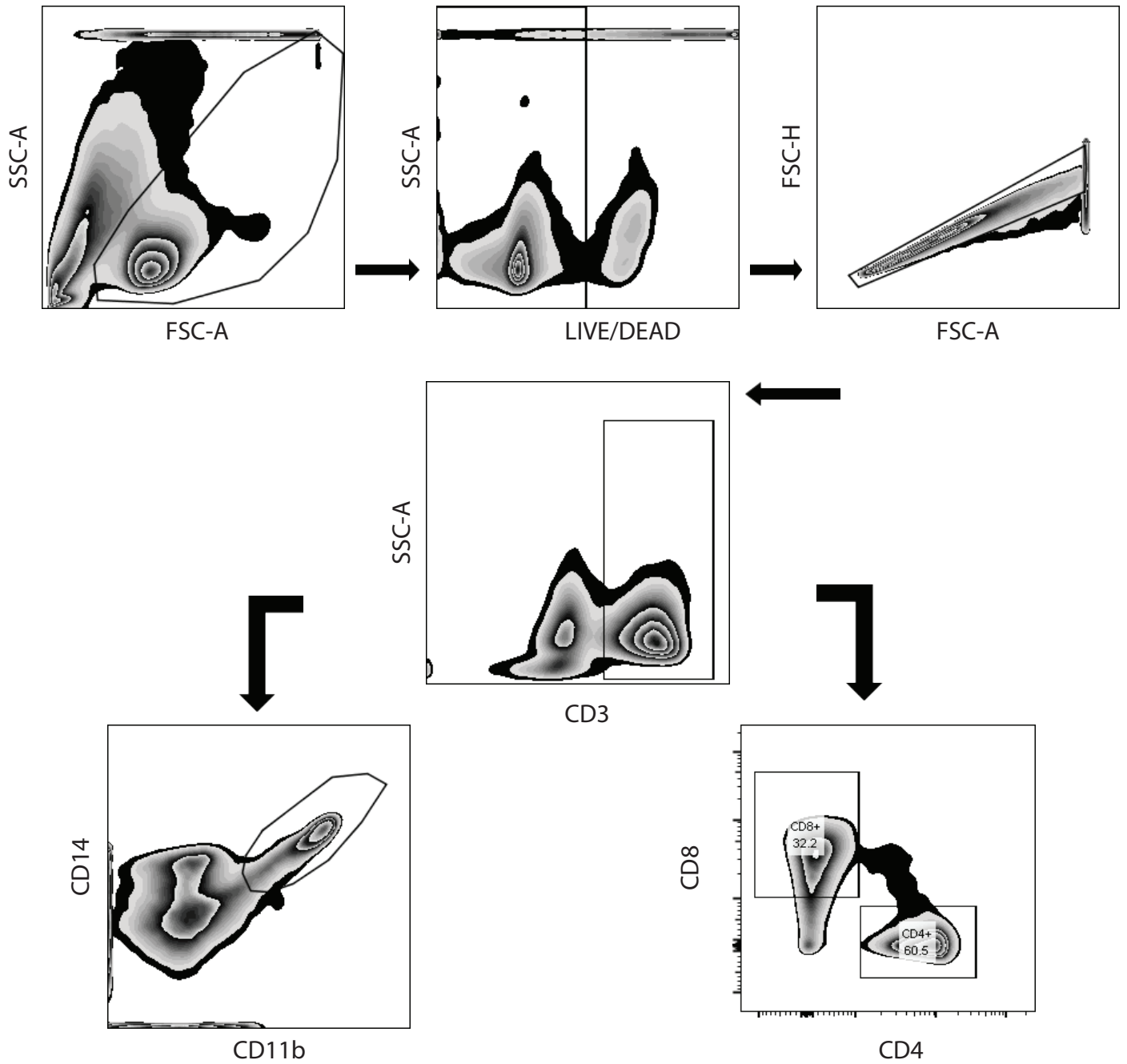


Figure 5–figure supplement 4: Hierarchical gating strategy used to identify lymphocyte and monocytic populations from decapsulated microspheres containing human peripheral blood monocular cells. Single cells were decapsulated from microspheres in 5mM EDTA, washed and processed for flow cytometry. First doublets were excluded from live cells, then cells were gated as CD3+ and CD3-. Subsequently, lymphocytes were further classified into CD4+ and CD8+, which are sub-categorized based on PD-1 staining. Double staining with both CD14 and CD11b defined macrophages, which were further analysed for PD-L1, CD80 and CD163 surface expression. All the antibodies and clone number are listed in the text and the key resources table.